Abstracts

Skin Printing

Anwar, Muniba[1], Boland, Thomas[2]
[1]Department of Bioengineering, University of Illinois at Chicago, Chicago, IL, USA
[2]Department of Bioengineering, Clemson University, Clemson, SC, USA

Introduction

Skin is the flexible, continuous covering of the body that separates the internal organs from the external environment. Besides covering the entire human body organs, it also serves to regulate the changes in the temperature, protects the body against sun, toxins and micro bacteria present in the environment, and keeps the fluid balance in the body.

As a safeguard of the body, in case of burn the most severely affected part of the body is skin. Alone in United States more than 2 million people in require medical treatment for burns each year, and between 3,000 and 4,000 die of severe burns. First degree burn only affect the top layer of the skin, second degree burn affects the top and middle layer of the skin i.e. dermis and epidermis, whereas a third degree burn which is the most severe burn affects all three layers of skin i.e. epidermis, dermis and fat layer. Usually, the sweat glands, hair follicles, and nerve endings are destroyed as well. This severe loss of skin can cause dehydration due to flow of fluids from blood to burned tissue. Infections can also complicate burn cases by spreading throughout the body and resulting in severe illness or even death. Skin grafting is currently the most common method to heal the burned skin. Grafting methods present today use unburned part of the skin in a patient, or animal skin, besides being painful it carries a risk of rejection.

The purpose of this research study is to make a skin substitute using gelatin and modified alginate that has mechanical properties close to that of human skin. By the process of inkjet printing this skin substitute can be tailored to be patient specific.

Materials and Methods

The gelatin and Alginate samples are made by printing 12% Alginate over gelatin of varying concentrations. Each printed scaffold has seven passes of Alginate and ten layers of Gelatin. The strength of the skin, and its mechanical properties change with age and the degree of the burn. The scaffolds use a different concentration of gelatin and alginate depending on the degree of the burn to match the mechanical properties of the scaffold as close to the persons' need as possible. The peak load and breaking point of the scaffold is found out by using tension compression testing machine, and a program called Test Works. The tension compression testing machine stretches the scaffold to their breaking point while the Test Works software plots the data, and enables the experimenter to find the peak load and young's modulus of the scaffold. To find out the amount of gelatin and alginate in the scaffold, a standard curve was made by using samples of varying gelatin and Alginate concentrations and performing BCA Protein Assay. The amount of gelatin is quantified by finding out the absorbance of each sample using a spectrophotometer, and a software called KC Junior which saves the data to a PC. After obtaining a standard curve, the absorbance of some unknown scaffolds are found by BCA Assay. Printing is done using HP Deskjet printer (HP 550C).

Results and Discussion

The results collected by BCA Protein Assay and spectrophotometer show the following relationship between percentage of gelatin in the scaffold and the absorbance. Figure 1 enables us to relate the absorbance of any sample to the percentage of gelatin that is needed to make that particular sample, whereas Figure 2 shows the stress strain curve of a 15% gelatin scaffold. The Young's modulus and elongation at break were found to be 16kPa and 17%, correlating well to Human skin, which has values of 8-10.2 kPa.

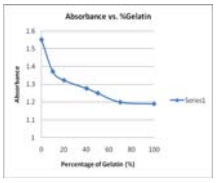

Figure 1.
The relationship between Absorbance and % Gelatin is shown in Figure 1 expected to be a linear relationship, but the cross linking of gelatin and alginate results in a decaying relationship.

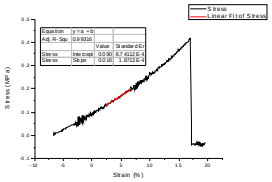

Figure 2. Stress-strain curve for a 15% gelatin scaffold.

Conclusions

All of this set up put together can help us print skin scaffolds for individual patients depending on the severity of their burn. The method of inkjet printing allows scientists to reproduce a specific shaped skin substitute using an HP Deskjet printer, and a simple imaging program such as Adobe. These scaffolds will eventually target burn victims that are in need of skin substitute, but they could also be used in cosmetology to remove scars.

References

Zahouani, H., C. Pailler-Mattei, and B. Sohm. "Characterization of the mechanical properties of a dermal equivalent compared with human skin in vivo by indentation and static friction tests." Skin Research and technology 15 (2009): 68-76.

Acknowledgements

NIH/NSF BBSI is acknowledged for funding provided under EEC 0609035. Special Thanks to Vipul Taneja for the scaffolds.

Using chloroperoxidase-latex nanoparticle conjugates to desulfurize diesel fuel

Joe Carver[1], John Barry, and Dr. Alexey Vertegel[2]
[1] Vassar College, Poughkeepsie, NY, USA
[2] Bioengineering Department, Clemson University, SC, USA

Introduction

Using biocatalysts to desulfurize diesel fuel is an emerging alternative to conventional hydrodesulfurization, which is expensive and energy intensive.[1] As conventional petroleum supplies dwindle and more marginal and sulfur-rich deposits come to replace them, the pre-combustion removal of sulfur compounds from fossil fuel – necessary to reduce the environmental impacts of fuel emissions – using these cheaper substitutes is becoming more desirable. However, to date biocatalysts have not been used on an industrial scale[2]. Among the primary difficulties are solubility and stability of enzymes in organic media; problems which have been solved, to some extent, by attaching the enzyme to nano- or mesoporous materials.[3,4] The goal of this project is to immobilize chloroperoxidase (CPO), which has been previously studied for its desulfurization capability[4], onto latex nanoparticles. Conjugation of chloroperoxidase with latex should improve both its activity and life-span in organic media.

Materials and Methods

Chemicals

CPO from *Caldariomyces fumago* was obtained from Colonial Scientific. 4% w/v 40 nm chloromethyl latex nanoparticles (NPs) and Alexa Fluor 594 were obtained from Invitrogen. Fluorescein isothiocyanate (FITC) and *N,N,N′,N′*-tetramethyl-*p*-phenylenediamine (TMPD) were obtained from Sigma Aldrich. Other chemicals were reagent grade and were not modified before use.

Conjugation of CPO with Alexa Fluor 594 and FITC

Both Alexa Fluor 594 and FITC were used to fluorescently label the enzyme before attachment to NPs. Separate samples of Alexa Fluor 594 and FITC were incubated with samples of CPO at 25° C for 90 minutes. Unattached Alexa Fluor and FITC dye was then removed using 10-KDa Microsep Centrifugal devices.

Conjugation of CPO and latex NPs

The purchased latex NPs were functionalized with chloromethyl groups, which can react with the amine groups of proteins to form stable covalent bonds. CPO and latex NPs were mixed and incubated overnight at 25° C.

Sizing of CPO-NP conjugates

Sizing of conjugates was performed using Dynamic Light Scattering (Brookhaven 90Plus).

Binding Efficiency Assay

Binding yield for CPO was assayed by measuring fluorescence at 590 nm for Alexa Fluor labeled enzyme and 528 nm for FITC labeled enzyme using a microplate reader. The enzyme-NP conjugates were centrifuged and the supernatant was collected. The fluorescence of the supernatant was used to calculate the binding yield. Alexa Fluor-CPO and FITC-CPO solutions with known enzyme concentrations were used as the standards.

Enzymatic Activity Assay

The activity of immobilized CPO and free CPO was tested using a slightly modified TMPD assay in aqueous media, as described previously[5]. As TMPD is oxidized by CPO in the presence of hydrogen peroxide it turns a deep, violet blue. Enzyme activity was measured by monitoring absorbance at 563 nm as a function of time using a microplate reader.

Results and Discussion

After attachment of labeled CPO, the average size of NP conjugates was 180 nm. However, size distribution data was bimodal, with the diameter for most of the particlesof 90 nm, with a small fraction of the particles with the diameter of ~400 nm.

Binding efficiency data from FITC-labeled samples was, on average, 18.9%, with a range between 15.0% and 25.9%.

A leaching assay of FITC-labeled conjugates showed very little separation of enzyme from nanoparticles, as would be expected for a covalent attachment. At 72 hours, enzyme leaching did not exceed 4%, indicative of high stability of the nanoparticle conjugates.

The TMPD activity assay of Alexa Fluor-labeled conjugates in aqueous media showed higher activity than free enzyme that had been prepared at the same time and stored at room temperature. Conjugates labeled with Alexa Fluor 594 had an initial reaction rate 24.5 times that of the enzyme in solution, and conjugates without fluorescent label showed a reaction rate 11.3 times greater than free enzyme. It is unknown why fluorescently labeled conjugates displayed higher activity. However, these results generally suggest that conjugation with nanoparticles improves the activity of CPO during storage. Fresh CPO from refrigeration storage (4° C) that was prepared just before the assay had a much higher initial activity than either of the conjugate samples; in fact, much of it reacted before the samples could be taken to the plate reader

Conclusions

CPO can be successfully conjugated to latex nanoparticles with improved stability as compared to free enzyme when stored at 25° C. Future work will focus on preparing the CPO-latex conjugates for use in organic media and ultimately test their efficacy at oxidizing sulfur compounds present in petroleum fuels.

References

1. Ayala, M., et al. (1998). Biocatalytic oxidation of fuel as an alternative to biodesulfurization. *Fuel Processing Technology* 57:2, 101-111.

2. Ayala, M., et al. (2007). The prospects for peroxidase-based biorefining of petroleum fuels. *Biocatalysis and Biotransformation* 25: 2-4, 114-129.

3. Bayramoğlu, G. et al. (2007). Covalent immobilization of chloroperoxidase onto magnetic beads: Catalytic properties and stability. *Biochemical Engineering Journal* 38: 2, 180-188.

4. Terres, E., et al. (2007). Immobilization of chloroperoxidase on mesoporous materials for the oxidation of 4,6-dimethyldibenzothiophene, a recalcitrant organic sulfur compound present in petroleum fractions. *Biotechnology Letters* 30:1, 173-179.

5. Kadima, T. and Pickard, M. (1990). Immobilization of chloroperoxidase on aminopropyl-glass. *Applied and Environmental Microbiology* 56: 11, 3473-3477.

Understanding Acetate Kinase Metabolism: The Search for Answers

Doucet, Tara, Cheryl Ingram-Smith, and Kerry Smith
Clemson University, Clemson, SC, USA

Introduction

Acetate Kinase (ACK: Eq [1]) is an essential enzyme in bacterial metabolism which uses ATP to convert acetate into acetyl phosphate which is then converted into acetyl CoA. In most bacteria, ACK partners with the enzyme phosphotransacetylase (PTA) to interconvert acetate and acetyl CoA (Eq [2]). Acetyl CoA is a central molecule in metabolism which exists in all domains of life without which organisms cannot break nutrients down into energy yielding molecules.[1] The two step equation which represents this process is:

(1) acetate + ATP ↔ acetyl phosphate + ADP
(2) acetyl phosphate + CoASH ↔ acetyl-CoA + Pi

Recently, ACK has been found in several pathogenic eukaryotic microbes, including the fungus *Cryptococcus neoformans* and the protist *Entamoeba histolytica*.[2] Most eukaryotes with ACK including *C.neoformans* and *E.histolytica* lack the enzyme PTA suggesting a novel role for the enzyme. Characterization of both the *C.neoformans* and *E.histolytica* ACKs has revealed novel biochemical properties. For example, the *E.histolytica* enzyme utilizes pyrophosphate (PP_i) instead of ATP as its energy source. Because ACK is present in many pathogenic microbes and is absent in plants, animals, or humans, it is an ideal drug target.

The best studied and modeled acetate kinase is the ACK which is present in *Methanosarcina thermophila* (a genus of *Archaea).* Therefore the *M.thermophila* enzyme was selected for recombination studied which would change single amino acid residues in the active site of the enzyme.

To investigate the unusual properties of the eukaryotic ACKs, amino acid residues are being altered in the *M. thermophila* (a genus of *Archaea*) enzyme. Subsequent changes in enzyme activity would indicate the importance of individual amino acid residues and assist in the development of a drug target for other ACKs in pathogenic organisms.

Materials and Methods

The hydroxamate assay was utilized to characterize the activity of the rMtACK variants. In 300 uL assays, reactants were added in the following concentrations: 100mM Tris- HCl [pH 7.5], 600 mM Hydroxylamine-HCl [pH 7] with varied concentrations of MgATP and acetate. Reactions were initiated by the addition of enzyme. The N211A, N211S, and N211T variants were added to a final concentration per reaction of 1.000 ug, 30.865 ug, and 4.905 ug respectively. After ten minutes, 600 uL of 5 % trichloroacetal acid, 1N HCl solution, and 1.25% $FeCl_3$ was added to terminate the reaction. Absorbance at 540 nm was read as a measure of acetyl phosphate formation.

In one set of reactions sodium acetate varied in concentration to determine the ideal concentration of the substrate. In subsequent assays the concentration of ATP- the phosphoryl donor- was varied to determine the ideal concentration of ATP for the variants. Each variant was tested independently.

Results and Discussion

Asparagine 211 was chosen for this study because it is indicated in the crystal structure to be a critical amino acid which helps to form the pocket for the adenosine ring of ATP. Asparagine 211 was changed to Alanine, Serine, and Threonine. The Serine and Threonine changes were made because they mimic the amino acid residues in equivalent positions in *C.neoformans* and in *E.histolytica* respectively.

It was found that the N211A variant yielded approximately a nine-fold increase in K_m and greater than a five-fold decrease in the K_{CAT} for acetate. The N211S variant yielded a seven-fold increase in K_m and a 235-fold decrease in K_{CAT} for acetate. The N211T variant yielded a twenty five-fold increase in K_m and a forty-four fold decrease in K_{CAT} for acetate. For all three variants tested, it was found that the K_m for ATP was raised approximately six to seven fold.

Conclusions

Because increased K_m suggests that kinetic affinity has decreased for an enzyme, it is clear that the changes affected catalysis. Results suggest N211 is important for both ATP binding and catalysis. Future work will include characterization of other variants in which other amino acid residues are examined.

References

[1]M. Campbell and S. Farrell Biochemistry (5th ed) Thomson Brooks/Cole 2006 .
[2] Ingram-Smith C, Martin SR, and Kerry Smith. "Acetate kinase: not just a bacterial enzyme." *Trends in Microbiology.* Vol. 14, Is. 6, pgs. 249-253. June 2006

Acknowledgements
Funding for the BBSI program was provided by NIH and NSF (EEC 0609035).
Technical advice was provided by Yu Meng and Matt Fowler

Optimization Of Wet Spinning Process To Make Carbon Nanotube (CNT) Fibers

Edwards, R[1], Sa, V[2], Satishkumar, R[3], Vertegel A[3], Kornev, K[2]
[1] University of Oklahoma, Norman, OK , USA
[2] Materials Science & Engineering, Clemson University, Clemson, SC, USA
[3]Bioengineering, Clemson University, Clemson, SC, USA

Introduction

Carbon nanotubes (CNTs) are known for extremely high tensile properties and very good electrical conductivity. The CNT fibers have a great potential in different applications as the materials for artificial muscles, supports for biomedical sensors and microelectrodes, etc.

Materials and Methods

Recently, we developed a wet spinning procedure to make these CNT fibers by loading CNTs with sodium alginate (1). Different types of CNTs were used. One of the main obstacles in preparation of CNT fibers is the homogeneity of CNT dispersion. CNTs are strongly bound by van der Waals forces making it hard to properly disperse CNTs in an aqueous solution. The procedure developed in Ref. (1) for SWCNTs cannot be directly applied for MWCNTs. We modified the procedure and used 0.5wt% MWCNTs and 2 wt% SDS and extended the sonication period to 3 hours (2, 3). We also studied different methods to optimize the dispersion process. The CNT concentration in alginate-CNT fibers was changed as 0.6 wt %, 1.2 wt %, 2.4 wt %, 12 wt % and 23.1 wt%. The alginate-CNT fibers were mechanically characterized on Instron (ASTM D3822). Their morphological characterization was done by scanning electron microscopy. Two hours sonication time was used to prepare SWCNT-SDS aqueous dispersion. Alginate-SWCNT fibers produced from this dispersion were compared with previously produced SWCNT fibers spun from 25 min sonication time SWCNT dispersion (1). Three hours sonication time was used to prepare MWCNT-SDS aqueous dispersion, as suggested in the literature (2, 3). The solutions were placed in a syringe and injected into a 15 wt/v % $CaCl_2$ coagulation bath at extrusion rate of 123.2 ml/hr. After 10 minutes in the bath, the fibers were transferred into a 3 wt/v% $CaCl_2$ solution. The fibers were air dried individually. A toxicity analysis was performed using a standard MTT Cell Proliferation Assay and a Live Dead Test. An overnight application of UV light was used to sterilize the fibers before application into a 12 well cell culture plate. Fibroblast cells were incubated with various fibers for a 24-hour period before testing.

Results and Discussion

The tensile experiments show that 25 min sonication gives better tensile properties of alginate-SWCNT fibers, implying that SWCNTs were damaged after excessive sonication. The tensile properties of the alginate-MWCNT fibers appeared worse compared to pure alginate fibers. This result assumes that the dispersion was not uniform causing many defects and bubbles in the fiber. The Scanning Electron Micrographs of the fiber surface shows grooves present along the fiber which implies stretching during the spinning process. The results of toxicity analysis show that all fibers with different CNT concentrations can be implanted into the connective tissue of the human body for further applications. Lower concentrations of SWCNTs demonstrated the most desirable results for cell survivability, while MWCNT fibers showed the same results throughout MWCNT concentration.

Conclusions

25 min sonication time results in the most homogeneous SWCNT-SDS dispersion. 3 hr sonication showed the best results for MWCNT-SDS dispersion. In overall, alginate SWCNT fibers demonstrated much better mechanical and anti-toxicity properties. Further studies need to be done to optimize the dispersion conditions resulting in fibers with better qualities.

References

1. Sa, V., and K. G. Kornev, *Material Research Society Symposium Proceedings, 1134*, 1134 (2009).
2. Jiang, L. Q., Gao, L., and Sun, J., *Journal of Colloid and Interface Science, 260*, 89 (2003).
3. Zhang, J., and Gao, L., *Materials Letters, 61*, 3571 (2007).

Acknowledgements

The author would like to acknowledge the NIH/NSF BBSI Program for their funding and support and also the members of Vertegel's lab, Konev's lab, Dr. Thomas Boland, and Sherri Morrison. The funding was provided under EEC 0609035.

Influence of Pigmentation and Twisting on Force Delivery of Orthodontic Elastomeric Chains

Fogle, J, Kennedy, M
School of Materials Science and Engineering, Clemson University, Clemson, SC, USA

Introduction: Orthodontists frequently use polyurethane chains as a force delivery system to close interdental space and to correct tooth rotations. These chains are generally manufactured by either die-stamping or injection-molding processes, and are sold in three different sizes: continuous, short, and long, all characterized by the lengths of connecter between circular modules. Previous studies have shown that the performance of the polyurethane chains can be influenced by temperature, extension, time of usage, self-life, and the oral environment itself.

Initially only produced in clear and grey, the chains are now available in a large array of colors to appeal to younger patients. These colors are produced by adding pigments/fillers to the polyurethane and can potentially change the mechanical response of the polymer.

This study is focused of the influence of pigmentation and single twists on the force decay and remaining force on teeth over the course of one hour. Twisting of the chain sometimes occurs due to the difficulty of stretching the chain ring over a much larger bracket and is depicted in Figure 2 below.

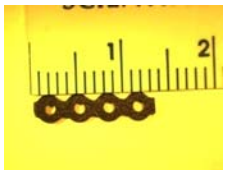

Figure 1: Optical image of purple Sunburst chain from GAC

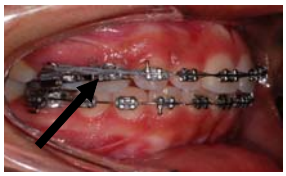

Figure 2: Elastic chain being used to derotate a bicuspid. Note the arrow pointed at the twist in the chain.

Materials and Methods: Three colors (clear, red, purple) of the short-module Sunburst Chain from GAC were selected for testing. Three samples of each color with and without a single twist were individually subjected to tensile testing using a Wagner FDIX 5 digital force gauge and FTK 100 handwheel test stand. Samples were cut to lengths of 4 rings with care taken not to cut too close to the circular module to prevent damaging the sample. The samples were connected to the test hooks by safety snaps removed from Eagle Claw Barrel Swivels size 5. Both of the test hooks were notched to secure the snaps and prevent torsion being applied to the sample during testing. Each sample was extended to a total length of 25 mm at room temperature (70 F) for 1 hr. The strain was noted by Brantely et al [2] to be the average length from molar to canine.

Results and Discussion: Figures 3 and 4 are load vs. time graphs produced from computed averages of each color tested. All samples experienced similar rates of force decay and deliver approximately the same amount of force during the test period. (˜ 650gf initial and ˜ 400 gf final) There was no significant effect of a single twist in the chains during the 1 hour test. The slight difference in final force between the two may be attributed to product variability of the 15 ft spool. The colored chains appear to be stiffer according to the graphs, likely due to a higher elastic modulus of the coloring additives.

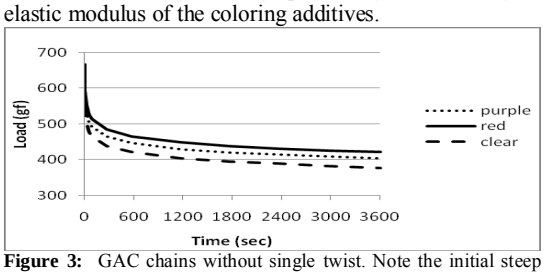

Figure 3: GAC chains without single twist. Note the initial steep decline in force at the start of the test and the similar rates of force decay for each color. Also, the colored chains generate higher forces than the clear indicating the additives make them stiffer.

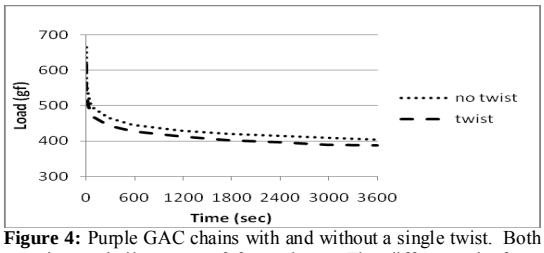

Figure 4: Purple GAC chains with and without a single twist. Both experience similar rates of force decay. The difference in force generated is not clinically significant.

Conclusions:

- Red and purple chains manufactured by GAC generate similar force levels as their clear standard chain.
- GAC red and purple chains experience force decay similar to the standard clear chain.
- The difference in flexibility of colored and non-colored does not appear to be clinically significant.
- Single twists have little influence on the force generated by the chain.

Future Testing: The Energy Chain from Rocky Mountain Orthodontics and the Colored Plastic Chain from American Orthodontics, all in clear, red, and purple, will be tested in the same manner as the GAC chains. Additionally, samples will be tested submerged in water maintained at 98 F for 1 hour to investigate performance in a simulated oral environment.

References:

1. D.L. Baty, J.E. Volz and J.A. von Fraunhofer, Force delivery properties of colored elastomeric modules,*Am J Orthod Dentofacial Orthop* (1994)
2. Brantley, W., & Eliades, T. (2001). *Orthodontic Materials: Scientific and Clinical Aspects*. Georgia: Georg Thieme Verlag.

Acknowledgements: BBSI, NSF grant EEC 0609035, J. Fuller of GAC, D. Ciarrocchi of RMO, E. Craig of AO, Dr. L. Fogle of MUSC

Optical Coherence Topography System Synchronization

Andrew Gosnell, Rui Wang, Joseph Zinkovich, Bruce Z. Gao
Clemson University, Clemson SC, USA

Introduction

Optical Coherence Topography is an optical signal acquisition and processing method using near-infrared light. Advantages include high-quality, micrometer resolution, three-dimensional images of live biological tissue. This image technique can penetrate deeper than confocal microscopy and with more resolution than ultrasound. The non-invasive, in-vivo imaging requires no staining or radiation that normally kills the sample. The current system is used to analyze chick embryos directly from the egg, focusing on the development of the heart valve from day 1. The study will lead to a better understanding of the human heart valve, and more importantly, how it can be recreated in a lab setting.

Principle

A near-infrared broadband light source is used to supply a short coherence length, which determines the axial resolution of OCT. The optical beam is sent through a beam splitter, which divides the light into two paths, one to the sample arm and one to the reference arm. The reflected lights from the two arms combine in the detector arm, when if they have the same length of optical path, interference can be measured. The interference light is induced into a spectrometer, in which a line-scan CCD camera records this interference spectrum. Taking Fourier transform to single line of the spectrum, a reflectivity profile at different depth (A-scan) within the sample can be obtained. A cross sectional tomography (B-scan) can be achieved by combining a series of depth scans (A-scan).

To achieve this three-dimensional image, the mechanical scanner and camera must be synchronized in order to record an image. A computer control program must be created to generate three waveforms to guide the laser and a camera trigger to record the scan. We made a control program to synchronize image acquisition in the OCT system.

Experiments and Methods

The synchronization program was successfully created and operated with the actual system. The NI PCI-6733 board was added to the computer hardware with the capacity to generate analog and digital channels. LabVIEW, a virtual instrumentation programming software, controlled the computer board. When running, three analog output waveforms and a digital trigger were generated. An externally added counter synchronized all channels. A Flat Sequence within a While loop allowed the channels to execute in a timed manner. In our system, the interference beam was sent to a custom-made high-speed spectrometer, consisting of a collimator with a focal length of 150 mm, a 1200 lines/mm diffracting grating, and an achromatic focusing lens with a focal length of 250 mm. The light spectrum was imaged onto the 2048 pixels of a line scan CCD camera capable of 18.5 kHz line rate. The B-scan OCT image consisting of 1200 A-scans corresponding to 3 mm was obtained by lateral scanning of the sample beam. The image reconstruction involved the following procedures: 1) The DC and autocorrelation terms were removed by subtracting the averaged spectrum of the recorded spectrum signal along the B scan; 2) The resulting spectrum signal was re-sampled into wave-number space; and 3) The OCT image was obtained by Fourier transforming the complex signal.

Results

Preliminary scans of a beating chick heart at day 2 were recorded. A hole was cut in the eggshell creating a window to the live floating embryo. In Figure 1, the straight white line across the image is actually the outer film of the egg yoke. Below the line appears to be developing heart, already beginning to divide into chambers.

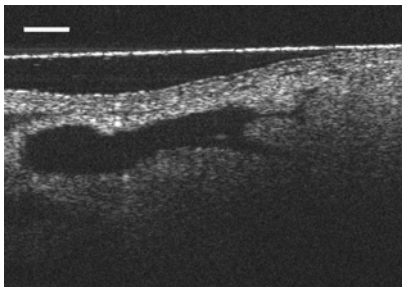

Figure 1: Chick embryo sample with heart in focus. Scale is around 200 micrometers.

Conclusions

Our results conclude that the developed synchronization program can be used with the current Optical Coherence Topography system to successfully scan live samples. This provides a tool that can systematically and accurately analyze live tissue, specifically the heart valve of a chick embryo, which will help continue more in depth research on the human heart. Future work will focus on finding ways to increase the speed of the scanning system.

Acknowledgements

National Institutes of Health and National Science Foundation
Bioengineering and Bioinformatics Summer Institute (EEC 0609035)
Clemson University Department of Bioengineering

Measuring Cell Growth on a Printed Bioscaffold

Hernandez-Cruz, L[1] ;Taneja, V[2]; Boland, T[2]
[1] Department of Biomedical Engineering, Texas A&M University, College Station, TX, USA
[2] Department of Bioengineering, Clemson University, Clemson, SC, USA

Introduction

For some time, researchers have been exploring the possibilities of using tissue engineering in medical applications. (Boland, et al) Tissue engineering is the process of generating tissues in a lab using a patient's cells. This process bypasses the immune system and solves the problem of the limited amount of donor tissues available. One form of tissue engineering that is being researched at Clemson University is cell printing. In cell printing, an inkjet printer is used to print cells, bioscaffolds, or both. The research done this summer was with respect to the bioscaffolds. Ideally, these bioscaffolds should promote cell growth. Using a metabolic assay, the number of live cells on a scaffold was tested. The higher the absorbance measured, the larger the number of cells in that well. This number was compared to the number of cells in media, without the presence of a bioscaffold. The hypothesis was that the scaffold would promote cell growth, producing a larger number of cells than the culture in just media.

Materials and Methods

In order to measure cellular response to the presence of scaffolds, cells first had to be cultured. The cells cultured were 3T3 fibroblasts. In order to work with these cells, some had to be thawed, others passaged. To actually quantify the growth of cells on the scaffolds, an MTS assay was performed with samples and controls.

To passage the cells, trypsin was used to detach the cells from the t75 flask in which they were cultured. After detaching the cells, they were centrifuged in a tube to separate the cells from the trypsin-media mixture. Next, the cells were resuspended using fresh media and counted using a hemocytometer. Once the cells were counted, they were divided among fresh t75 flasks as necessary. Once enough cells had been cultured, an MTS assay was performed to measure how well the cells grew on the scaffolds. To measure this, a twenty-four well plate was set up using three scaffolds cut into four pieces. There were two sets of controls and one set of negative controls. Every other day, measurements were made by adding sixty micro-liters of MTS reagent to three hundred micro-liters of media from the well and allowing it to culture for four hours. After four hours, three samples were drawn from each well to be tested and transferred to a ninety six well plate. The well plate was then inserted into a spectrophotometer to measure the absorbance at 490 nanometers. To create a standard curve, a single test was run using known amounts of cells in a twelve well plate.

Results and Discussion

A standard curve was derived by performing MTS on a known amount of cells and plotting the data. The overall trend on the data indicated that as the number of cells increased, the absorbance decreased. This is contrary to the original hypothesis that the increase in cell growth would increase the absorbance.

Figure 1: Sample of Gelatin-Alginate Scaffold

From the experiment, it was observed that the absorbance was higher in the control samples. When the standard curve data is taken into account, this means that there are fewer cells in the control samples than in the samples with the scaffolds. In Figure 2 below, this is shown more clearly. The error bars were derived by obtaining the standard deviation. For the scaffold, the standard deviation was 80000 cells, for the control, it was 15000.

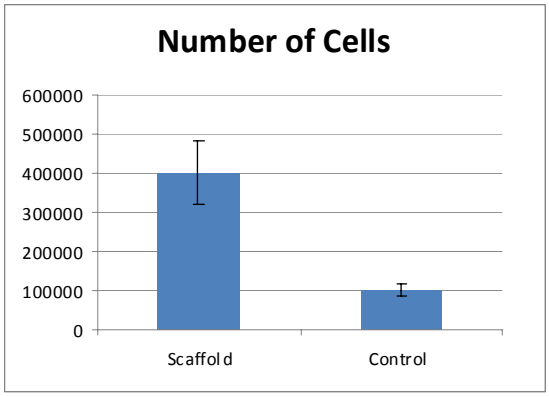

Figure 2: Number of cells on day seven

Conclusions

As predicted, the cells proliferated more in the scaffolds than on the culture plates alone. In the future, experiments should be done that measure cell proliferation over time so that the consistency of the results can be confirmed. The data collected can be used to determine the best way to make a scaffold to promote cell growth. As a result of these experiments, experience was gained in cell culture.

References

Boland, T., T. Xu, B. Damon, and X. Cui. "Application of Inkjet printing to tissue engineering." Biotechnology Journal 1 (2006): 910-17. Wiley Interscience. 28 Aug. 2006. Biotechnology Journal. 20 July 2009 <http://www3.interscience.wiley.com/cgi-bin/fulltext/112772254/PDFSTART>.

Acknowledgements

Bioinformatics Summer Institute program, its administrators, grant # NSF EEC 0609035, Vidya Seshadri

Formation of the Eastern Oyster Shell and Biomineralization

Korneva, A [1], Mount, AS[2]
[1] Emory University, Atlanta, GA, USA
[2] Clemson University, Clemson, SC, USA

Introduction

Research into biomimetics has expanded, feeding the growth of fields such as bioengineering and medicine. In nature, one can find materials that are much stronger, more elastic, more durable, more malleable, and overall more stress resistant than any synthetic material. As Nature prompts, the key to make durable and robust material lies in its composite and hierarchical structure organization. For example, the bricks in a wall are placed, not one on top of another, but the top brick is stacked on top of two bottom bricks. The idea is that if one pushes the wall in one direction, the bricks will be able to counteract the stress better than if they lay each on top of another, like in a domino. Biological structures are designed with a similar idea -they are able to counteract stresses in a variety of directions, more directions than a synthetic material can accomplish[1]. The success in nature is due to the stringent control that the cells have over the growth of the material. Cells are able to produce specific materials at the right time, and then switch and produce another compound until a specific composite is built. An example of such a material is the oyster shell: it is composed of crystals embedded in a pericellular macromolecular complex (PMC) whose microstructures provide it with extreme fracture resistance[3].

Most studies on natural composite shells have been carried out on nacre in pearl oysters. Nacre is an iridescent layer of mollusk shells, also called the mother of pearl. The shell that is so valued by craftsmen is composed of a brick-like arrangement of hexagonal platelets of aragonite and separated by sheets of organic elastic biopolymers. The non-organic part of the shell, aragonite, is a mineral made of calcium carbonate. This part provides conchoidal, or curved fracture pattern. This conchoidal fracture pattern is reinforced in another stress direction by the organic sheets acting in accord with the aragonite platelets to provide the shell with fracture resistance. Fracture resistance is a common feature of mollusk shells, like that of the Eastern oyster, *Crassostrea virginica*.

Materials and Methods

These studies were carried out on Eastern oysters. The Eastern oyster is a true oyster, excluded from the family of pearl oysters which produce nacre. This model organism utilizes the same principle of shell formation as the pearl oyster. First, the mantle organ of the shell deposits the periostracum, thus forming the outer layer of the shell[1]. This is followed by the formation of the prismatic layer, and then the nacreous layer in pearl oysters, or the PMC embedded crystals, both layers forming the inner shell [2,4]. We hypothesized that this biomineralization is strictly controlled by the epithelial cells of the mantle, which induces the migration of refractive hemocytes (REF)[4]. Hemocytes found in the PMC are believed to be directly responsible for the formation of the prismatic and inner foliated layer.

To prove/disprove the hypothesis, the Eastern oysters were kept in temperature, oxygen, and water conditions resembling their natural environment. The oysters were notched, and the next day their hemolymph was labelled with calcein AM ester and reinjected after one hour of incubation. The oyster shells were relaxed using a 30-35ppt magnesium chloride solution. Live relaxed mantle sections were dissected near the growing margin of shell. The mantle tissue was cut and visualized in the Nikon UDM, and Nikon AZ-100 microscopes using both FITC and epi-polarization channels, and confocal images were taken on the Nikon TI microscope. Scanning electron microscopy was also performed to better visualize the shell structures.

Results and conclusions

Our observations show that the formation of the *Crassostrea virginica* shell does involve hemocytes which directly result in the formation of the prismatic layer and the PMC layer of the shell. We believe that the prismatic layer together with the PMC are responsible for the superior mechanical properties of the shell. Also, these observations shed light on the mechanism of biomineralization: biomineralization can cause unwanted deposits on inserted medical devices, or can be desirable for certain implants such as the hip and knee joint implants where mineralization of a new bone is needed.

Acknowledgements:
NIH/NSF BBSI program as well as the U.S. Air Force Office of Scientific Research (AFOSR) Interfacial Surface Science Program, Grant FA9550-06-1-0133. The authors would like to thank Scott Streiker from the NEST lab at the University of Dayton and the staff at Clemson University Electron Microscope Facility and Advanced Materials Center, under the direction of Dr. Joan Hudson.

References:

[1] Calvert, Paul. "Biomimetic mineralization and biomineralization." Soft Materials. 7 Apr. 2007. Materials and Textiles Department University of Massachusetts. 20 June 2009. <http://tesumassd.org/faculty/calvert/papers/japanbiomim.pdf>.
[2] Carter, J.G., ed. *Shell microstructural data for the Bivalvia*. Skeletal biomineralization: patterns, processes and evolutionary trends, ed. J.G. Carter. Vol. 1. 1990, Van Nostrand Reinhold: New York. 297-411.
[3] Johnstone M.B. et al. "Cellular Orchestrated Biomineralization of Nanocrystalline Composites on Metal Alloys." In Press.
[4] Mount, A.S., Wheeler, A.P., Paradkar, R.P., and Snider, D. Hemocyte-mediated shell mineralization in the eastern oyster. *Science* **304**, 207-300 (2004).

Cross-Linking Effects of Printed Calcium Chloride with Alginate

Nelson, A. J.[1], Gao, M.[2], Boland, T.[2]
[1] University of Massachusetts Amherst, Amherst, MA, USA
[2] Clemson University, Clemson, SC, USA

Introduction

In the field of tissue engineering, electronic based methods are now used for precision placement of cultured cells in a variety of conformations. Specifically, modified computer printers are used to dispense quick drops of laboratory prepared bio-ink onto alginate-based scaffolds. To create the scaffolds, a blend of calcium ions and alginate chains cross-link and polymerize.

When calcium chloride interacts with dilute solutions of sodium alginate, a complex is formed between the divalent calcium ions and negatively-charged alginate segments. The segments of alginate are now linked, and the overall mechanical stability is improved. This makes for a great scaffold that can be used for attaching cells in a shell, tube, or cone formation. To achieve these different structures, alterations in the $CaCl_2$ solution is required.

The goal of this research project is to determine the effects on cross-linking between calcium and alginate with varying concentrations of calcium chloride. It has previously been determined that 2% alginate solution is ideal for visualizing the diffusion patterns of the printed calcium chloride. Also, concentrations of calcium chloride are best kept in the 0.1M and 0.5M to see specific images.[1] By correlating calcium chloride concentrations with the diffusion patterns in alginate, the formation of scaffolds used for cell printing can be specifically tuned towards a desired three-dimensional structure.

Materials and Methods

To observe the printing of $CaCl_2$ on alginate, a DeskJet 340 Monochrome printer was first modified. The outer casing and paper feed mechanisms were removed, and the printer was then mounted to a vertical standing optical board. The board was then mounted to an optical table with the microscope camera viewing system stationed underneath the track for the printer cartridge. The viewing system consists of a PixeLink PL-A781 Camera fixed to a linear three-dimension translation stage. To hold the slides that are printed on, a ninety degree pole clamp holds a pole extended to just underneath the cartridge track, but above the microscope.

Now with the printer and viewing system assembled, the microscope camera was connected to a computer and images were viewed using PixeLink Capture SE while video was recorded using PixeLink OEM software. Unlike a normal microscope, an external light source must be positioned so as to avoid contact with the printer, but also aid in the viewing of the printed calcium chloride.

Calcium chloride solutions were made at concentrations of 0.5M, 0.4M, 0.3M, 0.25M, 0.1M, and 0.05M. Added to these solutions was 300 µL of green food coloring to give the ink opaqueness. Each concentration was printed from an emptied 33 grade HP cartridge onto a thin layer of liquid 2% alginate. The alginate was manual applied to a microscope slide which was then positioned 5 mm underneath the cartridge track.

To create the printed patterns, the art function on Microsoft Word was used to make solid, dashed, and dotted lines. Each concentration was tested with each form of line. Images and videos recorded the diffusion with 10X magnification immediately after printing calcium chloride on alginate.

Results and Discussion

0.1M Dash 10X

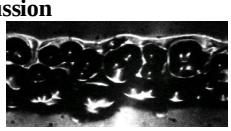

0.25M Line 10X

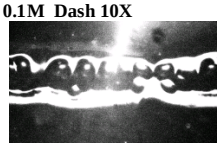

0.3M Line 10X

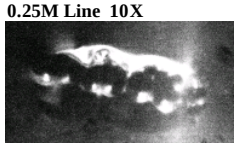

0.5M Dash 10X

As seen in the photographs above, the lower concentrations of calcium chloride do not form well-defined circles as the drops complex. Videos of concentrations lower than 0.3M show calcium chloride drops forming random shapes unevenly. The drops fully diffused and cross-linked in about 10 seconds.

The printing of 0.3M $CaCl_2$ solution shows the location of individual drops and their interaction among each other. There is still some uncertainty on structure at this level however. The 0.5M $CaCl_2$ exhibits the placement of single drops adjacent to each other while forming a three dimensional shell. Both the 0.3M and 0.5M solutions formed structures in about 5 seconds each. The 0.05M solution showed no significant complexes.

For future research in the area, it would be useful to quantify the extent of diffusion with a micro-scale grid system on the printing area. This then could give insights into how to best form a desired structure for cell printing scaffolds.

Conclusion

Results show a favoring towards higher concentrations of calcium chloride when cross-linking with 2% alginate. The lower concentrated solutions diffuse to a further extent than that of the higher concentrated solutions. The best concentration to view drop-drop interactions is 0.5M $CaCl_2$.

References

1.) Boland, T., Xu, T., Damon, B., Cui, X., "Application of inkjet printing to tissue engineering", Biotechnology Journal, 2006, 1, 910-917.

Acknowledgements

NIH/NSF BBSI for funding under EEC 0609035.
Department of Bioengineering, Clemson University
Vipul Taneja, Graduate Student, for
Laboratory Assistance

Printing Microvasculature in Skin Substitute

Roach, S[1]; Boland, T[2]
[1] Department of Biological Sciences, Clemson University, Clemson, SC, USA
[2] Department of Bioengineering, Clemson University, Clemson, SC, USA

Introduction

For the past 100 years, skin grafting has been the standard means of covering skin defects but these tissue constructs often fail engraftment because of inadequate blood supply. Survival of grafted tissues is dependent upon revascularization. Initial restoration of circulation appears to be due to linkage between existing graft and bed vessels, followed by an influx of host cells with a definite perivascular distribution. These findings have implications for skin autographs and tissue engineered skin substitutes[1].Organ printing has introduced a way of growing and maintaining blood vessels[2]. Our long –term objective is to develop thicker organs such as hearts and kidneys. Bioengineers think that it will be possible to print the entire network or arteries, capillaries, and veins that nature organs layer-by-layer. Our hypothesis is that organ printing has the capacity to penetrate nutrients throughout many layers of cells and will ultimately be the solution to donor shortages.

Materials and Methods

Endothelial cells have contributed to organ printing and skin graft neovascularization. These cells reduce turbulence of the blood flow allowing blood to be pumped further. Human microvascular endothelial cells (HMECs) were cultured for 7 days to enable nutrients to penetrate through the layers of skin. In this experiment, modified desktop printers are filled with suspensions of cells instead of ink. The printers are adapted by washing out the ink cartridges and refilling them with suspensions cells. A schematic diagram of the design used is shown below in Figure 1.

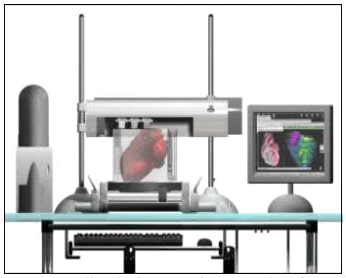

Figure 1: Cell Printing Hardware and Software[2].

The three technological steps of printing enabled us to create a functional human skin. Preprocessing was the first step and under this process, a blueprint was developed. It determines the localization of the cells within the 3D structure. We also developed what the main building block should be. It was determined that a drop on demand printing technique should be used. Step two, the processing stage, is when the actual printing took place. This occurred by a range of material transfer dispensing and deposition devices[2]. The endothelial cells were spun in a centrifuge and chopped forming tiny balls that flow like a fluid. The calls were loaded into a syringe-like nozzle on the printer and were spurted out into a ring. Between each ring was a layer of gelatin. This was continuously repeated until it created a tubular shape. When the gelatin relaxed, the cells merged together to form a smooth cylinder[2]. Lastly, postprocessing required the tissue construct to undergo maturity. To do so, the cells had to be placed in a wet environment such as a bioreactor so that they could become viable organs through the processes of maturity and differentiation.

Results and Discussion

This project has not yet been completed and currently, the only information available is that enough endothelial cells were grown to make a grid pattern which would later produce keratin skin (as seen in Figure 2). The modified alginate is nearly complete and will be added to the cells for printing. Printing will continue until the microvasculature renders a tube structure.

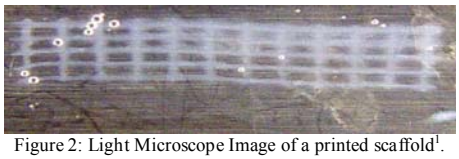

Figure 2: Light Microscope Image of a printed scaffold[1].

Conclusions

Due to this being an incomplete analysis, no conclusions can be drawn at this time. Future work will measure how long the cells remain viable in thick constructs at programmed porosity.

References

1. O'Cleallaigh S, Herrick SE, Bluff JE, et al. Perivascular cells in a skin graft are rapidly repopulated by host cells. *Plast Reconstr Surg* 2006; 60:864.
2. Mironov V, Visconti RP, Kasyanov V, Forgacs G, Drake CJ, Markwald RR. Organ Printing: tissue Spheroids as building block. *Biomaterials* 2008; 30: 2164-2174.

Acknowledgements

Funding was provided under EEC 0609035. Special thanks to Vipul Taneja and the Department of Bioengineering.

Modeling of Free Pulmonary Regurgitation and Analysis of Mock Circulatory System

KC Yeboa [1], Tiffany A. Camp MS, Tim Conover PhD[1],Richard S. Figliola
[1]University of Maryland Baltimore County, Baltimore, MD, USA
[2] Clemson University, Clemson, SC, USA

Introduction

There are various disorders which affect pulmonary circulation and thus pose a serious life jeopardizing threat to those afflicted. Pulmonary valve stenosis is a heart disease affecting the Pulmonary Valve in which outflow of blood from the right ventricle of the heart is obstructed. Another disorder is Pulmonary Atresia with which children are born without a functioning pulmonary valve or one which fails to open and close. Other children however are simply born without a Pulmonary Valve altogether and thus face free regurgitation of blood back into the right Ventricle.

With the previously mentioned disorders the malfunctioning Pulmonary valve is usually removed via surgical procedures and is then replaced often with bioprosthetic valves or the mechanical bileaflet heart valve, a mechanical heart valve usually made of carbon alloys which has two leaflets capable of opening and closing, simulating an actual valve. Disadvantages of bioprosthetic valves are that although effective in older patients they are not ideal for children in that they will repeatedly need to be replaced in the patient's lifetime. For the mechanical valve there is often overgrowth which hinders the motion of the leaflets as well as the fact that the patient must constantly take anti-coagulant drugs to prevent blood clots, effectively making patients hemophiliacs.

In Dr. Figliola's lab a fluid diode design was tested requiring no moving parts. Ideally this design will decrease Pulmonary Regurgitation to levels physiologically acceptable in the body while providing fewer complications than the other two options.

Materials and Methods

Testing was performed on the Mock Circulatory System in the lab designed to simulate pulmonary circulation and flow through the pulmonary artery. The system contains a ventricle pump chamber simulated by a flexible compliant rubber membrane. A timing box serves to create pulsation in the system simulating the pulsatile motion of blood flow through the circulatory system. The system contains a clear acrylic test section accurately modeled to resemble the pulmonary artery with its two branches leading to the lungs. There are large compliance chambers to simulate the capacitance experienced downstream of the pulmonary artery branches in the body. Tests were performed without a diode with the system running at a cardiac output of 5 L/min and a simulated pulse rate of 75 beats/min

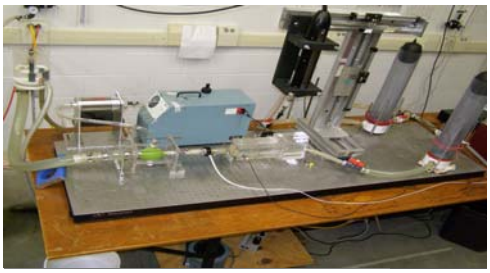

Results and Discussion

Adjusting the height of the head tanks it was found that as the Pulmonary Vascular Resistance increased so too did the regurgitant fraction increasing from about 1% to 33%, as resistance increased. Regurgitation through the pulmonary artery at a Pulmonary Vascular Resistance of 3, the value most similar to that found in the human body, was accurately modeled as well with results showing a 25% regurgitant fraction for a resistance of 3.

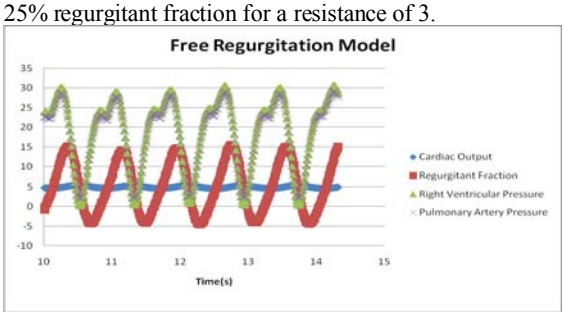

Conclusions

We successfully modeled free regurgitation through the Pulmonary artery while simulating the conditions found in the human body. In future testing the Mock Circulatory System will accurately be mathematically modeled so tests which do not have to be run real time can be taken to corroborate the real time data obtained.

References

[1.]T.A. Camp, K.C. Stewart, R.S. Figliola, 2007, "In Vitro Study of Flow Regulation for Pulmonary Insufficiency",**129,** pp284-287

[2.]J. Gohean, R.S. Figliola, T.A. Camp, T. McQuinn, 2006, "Comparative *In Vitro* Study of Bileaflet and Tilting Disc Valve Behavior in the Pulmonary Position",**128**,pp631-35

Acknowledgements

Thanks to NIH/NSF for providing funding under EEC 0609035. Thanks to BBSI for providing the opportunity and guidance for this research.

Biochemical Cues for Adipose Tissue-Derived Stem Cell Differentiation in Diabetes

Zhang, HS, Simionescu, D, Simionescu, A,
Clemson University, Clemson, SC, USA

Introduction

There are 23.6 million children and adults in the United States, or 7.8% of the population, who have diabetes. Diabetes is a major risk factor for cardiovascular diseases and diabetics have as much as a 2 to 4 times greater frequency of cardiovascular disorders. As a consequence, diabetics are more prone to undergo surgery for repair or replacement of tissues such as blood vessels and heart valves. Tissue engineered constructs based on scaffolds and autologous stem cells are currently being developed, but very little information exists regarding the fate of tissue engineered devices in the compromised patient, and more specifically in diabetic environments. Diabetes is characterized by elevated levels of blood glucose, which interacts irreversibly with proteins, lipids and nucleic acids via oxidation and cross-linking processes, resulting in formation of advanced glycosylation end products (AGEs). Glycoxidation induces severe cell and matrix alterations that result in endothelial dysfunction, accelerated atherosclerosis, activation of inflammation, fibrosis, impaired healing and ectopic calcifications, all of which are not conducive to the desired integration and remodeling of tissue engineered constructs. Adipose-tissue derived stem cells (AdSCs), until recently an underappreciated cell source for tissue engineering, show excellent potential for use in cardiovascular tissue engineering. The overall aim of this project is to evaluate the differentiating potential of diabetic stem cells compared to "normal". Our hypothesis is that diabetic conditions alter adipose stem cell differentiation.

Materials and Methods

Rat AdSCs were obtained from normal and diabetic (STZ-treated) rats by lipectomy and cultured. Diabetic stem cells were maintained and propagated in culture in Diabetic Medium (DMEM, 10% FBS, 550 mg/dl Glucose) while normal cells were maintained in same conditions at normal glucose levels (100 mg/dl). These cells were then split into 20 6-well plates, varying in differentiation media. The five types of media used for both normal and diabetic cells include: Osteogenic Media **(OM)**, Adipogenic Media **(AM)**, Chondrogenic Media **(CM)**, Myofibroblast Cell Media **(myoFB)**, and Endothelial Cell Media **(ECs)**. After being cultured for 2 weeks while changing the media every 3-4 days, specific staining was performed. Von Kossa, Alcian Blue, and Oil Red O were used and immunofluorescence on the myofibroblasts and endothelial cells. MMP activities in cell extracts were measured by gelatin zymography.

Results and Discussion

To evaluate their multi-potency, **diabetic AdSCs** were exposed to specific agents and growth factors to induce their differentiation into specific lineages including: *endothelial cells, myofibroblasts, chondrocytes, osteoblasts and adipocytes* (**Fig. 1**).Diabetic AdSCs expressed less CD31 and eNOS when exposed to endothelial cell differentiation media, suggesting that endothelial regeneration may be difficult in diabetes. On the other hand, diabetes stimulated formation of actin-positive cells when exposed to myofibroblast-inducing media. Diabetic AdSCs, when grown in diabetic media expressed very high levels of N-(carboxymethyl)lysine (CML)-positive proteins indicating that cells maintained high levels of protein glycosylation and AGE products. Diabetic stem cells also produced less GAGs and collagen type II in CM media, indicating that use of diabetic stem cells for cartilage regeneration may be impaired. Von Kossa staining indicated the presence of more osteoblast-like cells among the diabetic cells compared to normal cells. MMP activities were reduced in diabetic cells. Less evident differences were noted between normal and diabetic stem cells as far as adipogenesis was concerned (**Fig. 1**).

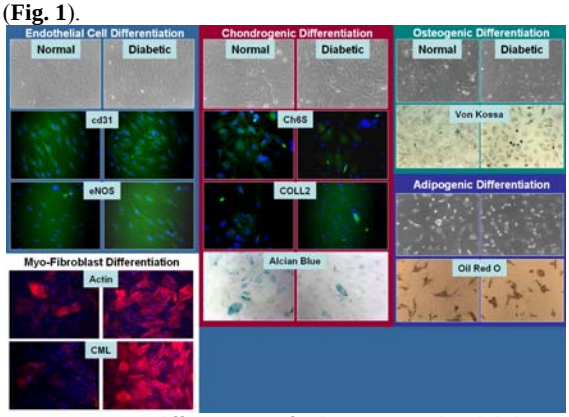

Figure 1. In vitro differentiation of AdSCs in normal and diabetic conditions. Grey pictures are phase contrast images; CD31, eNOS, Ch6S, COLL2 = immunofluorescence green with blue nuclear DAPI stain; actin and CML are red with blue nuclear DAPI stain. CML = carboxymethyl-lysine (an AGE marker of glycoxidation); Ch6S = chondroitin-6-sulfate; COLL2 = collagen type II.

Conclusions

(1.) Biochemical stimuli successfully differentiated normal and diabetic AdSCs into their respective phenotypes: osteoblast-, adipocyte-, chondrocyte-, myofibroblast-, and endothelial-like cells. **(2.)** Normal and diabetic stem cells exhibit different abilities to differentiate *in vitro*. **(3.)** Reduced MMP activities in diabetic cells also indicate differences in migration potential when compared to normal cells.

Acknowledgements

Funding was provided under NSF grant EEC 0609035. Thanks go out to the BBSI program at Clemson University and the entire BTRLab family.

Cell Seeding of Heart Valve and Vascular Scaffolds: Tissue Engineering in Diabetes

Maivelett, J, Simionescu, A, Simionescu, D.
Clemson University, Clemson, SC, USA

Introduction

Diabetes increases the risk of cardiovascular disorders by 2 to 4 times and therefore increases the frequency of heart valve and blood vessel replacement.[1] Little, however, is known of the effect of a diabetic environment on tissue engineered devices.

The purpose of this study was to determine the best method of cell seeding tissue engineered heart valves (HVs) and vascular grafts (VGs), to discern the effect of a diabetic environment, and to examine the effects of Penta-Gallolyl-Glucose (PGG) fixation.

In this study, HVs and VGs were seeded with rat adipose stem cells (RASCs) from normal and diabetic rats, and were subjected to normal and diabetic environments respectively. Scaffolds were also fixed with PGG, a matrix stabilizing agent, and its effects were compared to non-PGG controls.

Materials and Methods

RASCs were obtained from normal and diabetic rats (induced with streptozotocin) and cultured in normal (1 g/L glucose) and diabetic (4.5 g/L glucose) media, respectively.

Fresh porcine aortic HVs were retrieved from a local abattoir, cleaned, decellularized by detergents and treated with 0.075% PGG solution overnight. Valve cusps were loaded with cotton balls soaked in PGG solution to obtain desired cusp arrangement, coronary arteries were sutured, and valves mounted to Silicone aortas. Valves were then seeded with normal or diabetic cells by one of two methods: a combination of vacuum and chemotaxis, or a combination of injection and chemotaxis. Cells were added to the arterial aspect of the cusps and vacuum was applied from the ventricular aspect in a sterile filtering unit. Cells were injected in between the layers of the cusps using a hypodermic syringe. Chemotaxis was achieved by placing cotton balls soaked in 100% fetal bovine serum (FBS) on the ventricular side of the valves. Once seeded, the valves were mounted in the Clemson Heart Valve Bioreactor for 5-10 days at 37℃ in the appropriate media. Rates of 20 and 40 bpm were used in the first two days and a rate of 60 bpm was used thereafter. Valve cusps were examined by Live/Dead, MTS, and histology stains (H&E, Movat) for proper cell adhesion and survival.

Fresh carotid arteries were obtained from Animal Technologies Inc, cleaned, and decellularized in 0.1 M NaOH at 37℃ for 24 hours. PGG arteries were treated with 0.075% PGG solution at room temperature overnight. Arteries were mounted to Luer-lock connectors and zip ties were used to secure the arteries in place. Syringes were used to fill the arteries with appropriate cell type, connector ends were capped, and the arteries were subjected to vacuum in a sterile filtering unit for 10 minutes. Arteries were then placed in 100% FBS overnight at 37 ℃ to induce outward chemotaxis. The arteries were mounted in the Clemson Vascular Bioreactor for 5-10 days in appropriate cell media. Flow rates of 20 and 40 mL/min were used for the first two days and a rate of 60 mL/min was used thereafter. Once removed, arteries were examined by Live/Dead assay, MTS assay, and histology stains (H&E, Movat) for cell analysis.

Results and Discussion

The diabetic scaffolds seemed to have more cells present on Live/Dead, histology, and MTS. Therefore, the diabetic environment seemed to increase cell proliferation.

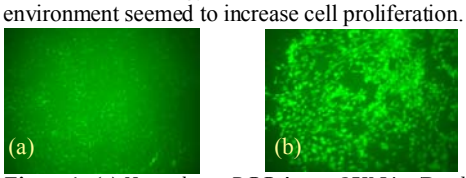

Figure 1: *(a) Normal non-PGG Artery 25X Live/Dead (b) Diabetic non-PGG HV Cusp 100X Live/Dead. Green fluorescent dots are live cells.*

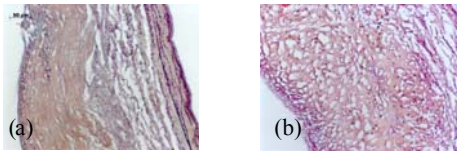

Figure 2: *(a) Normal non-PGG HV Cusp 200X Movat (b) Injected Diabetic non-PGG HV Cusp 200X Movat. Collagen is yellow, elastin dark purple/black, and nuclei blue/black.*

The reason for this is not fully understood, but is believed to be linked to the higher glucose content, which may provide more sustenance for cells and thus allow them to proliferate faster. PGG is a known matrix stabilizing agent. It is, however, slightly toxic.[2] Non-PGG fixed scaffolds contained more cells versus their PGG counterparts. This trend was visible in both Live/Dead and histology. This toxicity, however, is a willing sacrifice for the amount of stabilization PGG provides. Also, the slight degree of toxicity may help to prevent contamination of the tissue. Contamination was an issue with the bioreactors. The PGG scaffolds, however, showed no or less contamination than non-PGG controls. For HV cusps, cell infiltration was inconsistent through vacuum and more consistent through injection. Injection, however, caused visible damage to the cusps in histology. VGs were successfully seeded on the surface with signs of outward cell infiltration.

Conclusions

Decellularization was successful and tissue structure maintained. PGG scaffold stabilization lowered cell count, but increased contamination resistance and stability. Cell seeding of arteries through vacuum and chemotaxis proved successful, while injection was the best method for valves. Cell distribution was improved after bioreactor conditioning. The diabetic environment increased cell proliferation rate. Further studies, however, are warranted.

References

[1] "Diabetes and Cardiovascular Disease." American Heart Association. 19 July 2009 <http://www.americanheart.org/presenter.jhtml\identifier=3044762>.

[2] Chuang, Ting-Hsien, et al. Polyphenol-Stabilized Tubular Elastin Scaffolds for Tissue Engineered Vascular Grafts. *TISSUE ENGINEERING: Part A* **15**, 2009.

Acknowledgements: The authors would like to thank NASA/SSBR SC Space Grant Consortium and NIH Grant HL084194 for funding this research experience.

3-D Image Reconstruction of Aortic Aneurysms for Real-Time Biomechanical Analyses

McCaskill, B , and Nagatomi, J
Department of Bioengineering, Clemson University, Clemson, SC, USA

Introduction: An aneurysm occurs when the terminal aorta permanently dilates to dangerous proportions, risking rupture[1]. Without proper screening and prevention, these aneurysms will burst and cause massive internal bleeding. They occur in two main areas: in the brain and in the thoracic and abdominal aortas. Aneurysm rupture is a mechanical failure of the degenerated aortic wall and is a significant cause of death in developed countries[1]. Advanced screening techniques for their severity based on biomechanics can, however, reduce the mortality of abdominal aortic aneurysms[2]. In order to properly assess the mechanical behaviour of the aneurysm tissue it is necessary to examine the relationship between the internal pressure and surface curvature changes[2]. The long-term goal of the present study is to develop a novel device that allows real-time measurements of 3D surface geometry of small animal aortas subjected to inflation. To pursue this goal, we are currently developing an image processing program to reconstruct a 3-D model from 2-D projection images of the vascular tissue.

Materials and Methods:

Phantom Images: A large scale imaging phantom to model aneurysm was constructed out of a PVC pipe (2" diameter) with electric tape. A multitude of projection images at small angle intervals of 10 and 15 degrees were taken with a Nikon D40X camera with attached Nikon Speedlight SB600. These projection images (Figure 1) were then imported into MATLAB for gray scale conversion, edge detection, and image fill using holes.

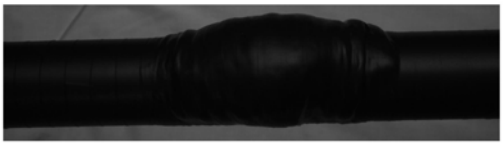

Figure 1: Projection Image of Aneursym Model

Figure 2: Black/White Segmentation using MATLAB

MATLAB Code: A MATLAB code was written using the image processing demo package. A script called Detecting a Cell Using Image Segmentation served as a basis for our custom batch image processing code to convert gray-scale images (Figure 1) into the final segmented images (Figure 2) for all angles.

The final part of the coding was used to help visualize a model of the projected images in 3-D space. This was done by constructing a 3-D volumetric box of zeros and ones. The whole box was coded as ones, while each image was projected (at the same angle at which the image was taken) through the box to create the zeros where the aneurysm lay in 3-D space (Figure 3).

Results and Discussion: All of the images were run through the MATLAB coding for batch image processing with black and white segmentation. These images were all successfully segmented, and the 3-D model was also

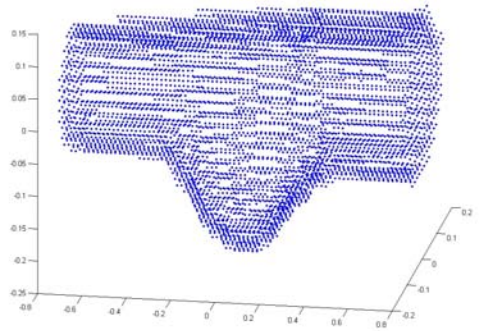

successfully created.

Figure 3: 3-D Model from Processed Images

Conclusions and Future Studies: The ultimate goal of the project is to develop a novel testing device that allows for inflation and real-time strain measurement of a small diameter vascular tissue. Thus, similar MATLAB coding will be used to construct a 3-D model of the vascular tissue under real-time pressure from the gray scale images. Minor adjustments may be necessary to compensate for the different image sizes and the image to image variability with segmentation. The inflation testing device with real-time strain measurements will consist of: a specimen chamber to keep the tissue hydrated, rotating connectors to achieve the small angle intervals, and a syringe pump with gauge and tubing to provide a constant pressure to the vascular tissue. Finally all of these parts will be interfaced with the imaging device (a dissection microscope with attached camera) for collection of images and analysis.

References: [1] Vorp, David A. "Biomechanics of Abdominal Aortic Aneurysm." *Journal of Biomechanics* 40 (2007): 1887-1902.

[2] Sacks, Michael S. "In Vivo Three-Dimensional Surface Geometry of Abdominal Aortic Aneurysms." *Annals of Biomedical Engineering* (1999): 469-479.

Acknowledgements: The authors would like to thank Dr. Bruce Gao and Dr. Delphine Dean of the Clemson Bioengineering Department and Dr. Brian Dean of the Clemson Computer Science Department for their help with the image processing and MATLAB coding. The authors would also like to thank NASA, specifically the SC Space Grant Consortium, for research funding.

Characterization of Semi-synthetic Collagen/poloxamine hydrogel containing hyaluronic acid for 3D Bladder Smooth Muscle Cell Culture

Ostendorff, R. and Nagatomi, J.
Cell Mechanics and Mechanobiology Laboratory, Department of Engineering
Clemson University, Clemson, SC 29634-0905

INTRODUCTION

Diabetes affects over 23.6 million Americans and is the fastest growing epidemic today. Over half of diabetics experience bladder dysfunction which can lead to long-term complications. Symptoms of diabetic bladder dysfunction include decreased sensation, reduced contractility of bladder muscle, and inability to completely void. These symptoms can lead to over-distension of the bladder walls which is thought to cause a change in cellular function. The abnormal mechanical environment the bladder smooth muscle cells are subjected to is thought to trigger phenotypic shifts. Previous research has shown that SMCs subjected to a sustained tension in 3D culture exhibit an increased expression of α-smooth muscle actin, a contractile protein, and an elongated morphology in the direction of tension when compared to no tension SMCs[1]. A custom-made computer-controlled bioreactor was designed and constructed to further investigate the effects of static and cyclic tension on 3D SMC cultures. A novel hydrogel formula was developed to create a 3D culture milieu with optimum mechanical strength and pore architecture for cell spreading. The present study investigated physical properties of the hydrogel system. Specifically we examine the effects of varying content of hydrogel component, hyaluronic acid (HA), on the swelling ratio and tensile mechanical behaviours.

MATERIALS AND METHODS

Preparation of Tetronic T1107-acrylate/collagen/ hyaluronic acid hydrogel for 3D SMC culture

A four arm PEO-PPO block copolymer (Tetronic T1107, BASF, Evans City, PA) was acrylated to allow photopolymerization. T1107 powder was dissolved in toluene and azeotropically distilled. After toluene was boiled off, T1107 was dissolved in dehydrated dichloromethane and mixed with triethylamine on an ice bath while stirring. Acryloyl chloride was added dropwise over a 2 hr period and the reaction was run in a cold room while stirring for 24 hrs. The product was precipitated in ethyl ether and washed to neutralize; this was followed by 3 more ether precipitations. The final product was dried under vacuum overnight and stored in -20 °C freezer. 3D cultures were made by dissolving T1107-acrylate and type-I collagen (MP Biomedicals, Solon, OH) in 0.02N acetic acid solution, resulting in 5wt% Tetronic and 0.5wt% collagen concentrations. Photoinitiator, Irgacure 2959, was added in 0.05wt% to the Tetronic-collagen solution and incubated in 4°C for 30 min. Varying concentrations of HA (0.10wt%, 0.15wt%, 0.20wt%) were added to solutions and quickly neutralized with NaOH in custom made Teflon molds (3x1x0.3 cm wells). Varying amounts of PBS solution were subsequently added to neutral hydrogel solution to adjust the final concentration and volume. The hydrogel strips were cast with 1x0.5cm porous BioVyon wafers (Porvair, Norfolk, UK) containing steel pins to hold wafers in place. Cultures were allowed to incubate for 30 min (37°C, 5% CO_2) and then a layer of mineral oil was applied to the top of the gels to keep from dehydration. Gels were cured under 365nm UV light for 10 min.

Mass Swelling Ratio

Hydrogel samples containing collagen, T1107-acrylate, and varying levels of HA were cast (n=4 per group). The rectangular gels were equilibrated in 10% PBS solution for 24 hr to remove unpolymerized monomers. Samples were lyophilized and dry weights (W_d) were recorded. Samples were immersed in distilled water, allowed to swell for 24 hr and wet weights (W_s) were recorded. Mass swelling ratio, q, was calculated by ratio of wet to dry weight.

Tensile Testing

Hydrogel samples containing varying amounts of HA were loaded into MTS Synergie 100 (MTS Systems Corporation) by wafers. Distance between loading cells was recorded. The samples were subjected to uniaxial tensile loading at a rate of 5mm/min until breaking point and force and elongation data were collected using TestWorks 4 software.

RESULTS

Swelling tests showed a slight increase in mass swelling ratio with an increase in HA content. Stress-strain behaviour from tensile testing showed a general trend of increased stiffness and elastic modulus as HA content increased. Analysis of peak stress showed that gels with 0.10% and 0.15% HA content were not significantly different, and exhibited a much lower peak stress than 0.20% HA content gels. Analysis of peak strain showed that 0.10% HA content gels exhibited a much higher peak strain than 0.15% and 0.20% HA content gels, which were not significantly different.

DISCUSSION AND CONCLUSION

The increase in mass swelling ratio with increased HA suggests that HA expands hydrogel pore size to allow for increased water uptake. Tensile testing showed a general trend of increased stiffness and elastic modulus when analysed with linear stress-strain model assumptions. Peak stress and strain trends show that an increase in HA content provides strength for the gels while compromising elasticity. Results suggest that an increase in HA, and thus a decrease in PBS content, causes greater water uptake that results in a construct which can withstand a greater amount of applied tension than gels with lower HA contents. Further research includes cell viability testing, cell morphology analyses with confocal microscope, cell functional analyses, and exposure of cells to varying levels of static and cyclic tension with custom bioreactor.

ACKNOWLEDGEMENTS

Authors would like to thank NASA (SC Space Grant Consortium) for funding; Ms. Eunhee Cho, Mrs. Rebecca Cribb, and Mr. Vincent Friebe for their help and advice.

REFERENCES

[1]Roby, T., et. al. 2008. "Effect of Sustained Tension on Bladder Smooth Muscle Cells in Three-Dimensional Culture."

The Effect of 8 Gy Single Dose Whole Body Irradiation on Osteoclast Activity and the Resorption of Bone

Powell, S., Smith-Sielicki, H., Bateman, T.
Clemson University, Clemson, SC USA

Introduction

Radiotherapy is used to treat patients with various types of cancer. Nearly half of all cancer patients are treated with radiation therapy[1]. Generally, patients are treated with a dose of radiation ranging from 50 to 80 Gy. When treating patients with extreme doses of radiation, there are many adverse effects that result from exposure. The most common effects include the increased loss of bone density which results in an increased fracture risk. These effects lead to other complications, such as osteoradionecrosis, which is the death of bone tissue[2]. Exposure to radiation is also known to increase osteoclast activity, which leads to an increased rate of bone resorption. As osteoclast activity increases, more bone is resorbed than is created. As a result, there is a net loss of bone. In order to better understand the effects of radiation exposure on bone, this study investigates the extent to which a large, single dose of radiation has on the activity of osteoclasts and the overall resorption of bone. It is expected that mice irradiated with an acute 8 Gy dose of radiation will have a smaller amount of bone present, more osteoclast activity, and thinning of the trabecular struts.

Materials and Methods

Twenty-four mice were five weeks old upon arrival, at which point the mice were isolated and were allowed to acclimate for a period of one week. Following the isolation period, the mice were divided into four different groups based upon their weights. Each group was comprised of animals resulting in an average weight that was very similar to the overall average weight of all of the animals. The four groups consisted of two day irradiated, two day non-irradiated, six day irradiated, and six day non-irradiated. The irradiated groups were exposed to a single, whole-body acute X-ray dose of radiation (8 Gy). All mice were closely monitored throughout the remainder of the study following radiation exposure. At two days post irradiation, twelve mice (6 irradiated and 6 non-irradiated) were euthanized, at which point blood and right and lefthind limbs (tibia and femur) were collected for further study. The same procedure was performed at six days post irradiation on the remainder of mice. Following the collection of the hind limbs, the tibiae were subjected to micro-computed tomography (microCT). Analyses were performed to determine the bone density and the trabecular morphometry of all samples.

Histology was also performed on all tibiae after the micro-computed tomography analyses were complete.

Serum chemistry was also performed on all blood samples collected. Two different assays were performed, which detected tartrate-resistrant acid phophatase-5b (TRAP) and osteocalcin. TRAP is a serum marker for bone resorption, while osteocalcin is a serum marker for bone formation.

All tibiae were prepared in paraffin and sectioned. After preparation, all sections were stained with acid phosphatase, indicating the presence of osteoblasts, and TRAP5b, indicating the presence of osteoclasts.

Results and Discussion

Following microCT analyses, the internal trabecular morphometry of all tibiae were examined. Each irradiated group was compared to the non-irradiated control group for the same post-irradiation time point (2-day or 6-day). Within the two day comparison, the irradiated mice were observed to have more bone than the non-irradiated mice. This was unexpected, due to the contradiction with the findings of previous research. While the irradiated samples contained more bone, the TRAP assay indicated more osteoclast activity in the non-irradiated mice. Trabeculae were more numerous and thicker in the irradiated mice, while also being closer together, resulting in an overall increase in the strength of the bone. It is know that trabecular struts diffuse stress throughout a bone sample, creating stress concentrations at various sites throughout the bone. Radiation exposure results in trabecular struts become thinner and less abundant, the risk of fracture increases. This is one of the adverse effects of radiation treatment. As for the comparison between the six day mice, the results were what were expected from the hypothesis. The irradiated mice had much lower bone densities and fewer trabeculae. These trabeculae were thinner and more spaced out compared to the non-irradiated mice.

Using SigmaStat, it was determined that the difference between the Connective Density in the two day mice was not significant enough to reject the possibility of random chance. However, the difference was significant enough in the six day mice. Further study is needed to investigate why the two day irradiated mice had more bone than the non-irradiated. Future studies could investigate the same objectives but include a subject group at three days along with the two day and six day groups.

Conclusions

It is confirmed that radiation increases the presence of osteoclasts. It has been anecdotally noted in previous studies that a slight increase in bone occurs in such short time spans with irradiated mice immediately after exposure. However, this is the first study showing a significantly larger amount of bone in irradiated mice in a short time period following exposure. At this time, the proper mechanisms cannot be proposed for this occurrence. Further studies are needed to determine this.

References

1. Hall, EJ "Radiation, a two-edged sword". (2000)
2. Donovan, D.J., et al. "Osteoradionecrosis of the cervical spine" (2005)

Acknowledgements

Thanks for NASA Life Grant for funding the research project. Thanks to Jeff Willey and Eric Livingston for helping throughout the research project.

Flow cytometry of cells with laser guidance and digital imaging

Smalls, AP, Department of Bioengineering, Clemson University, Clemson, SC, USA

Introduction

Cell analysis by flow cytometry has become one of the new innovative ways of analyzing cells in vivo. Flow cytometry is a method to examine, sort and count cells moving in a fluid stream. Improvements to the flow cytometers are being researched because the process can sometimes change the characteristics of the cells. To help minimize the change in characteristics research is being done in different areas of the process. Some of the current innovations include better fluid focusing with changes in chamber designs. It was found that the particles spread out and were hard to detect and called for correction due when tight flow focusing was not present causing a variation in velocity of the particles. Quantum dots are another method that has been used for better multispectral analysis. Previous methods that use traditional reagents have a large range of emissions that are excited at different wavelengths. Quantum dots make detection easier because they can be excited at any wavelength less than their emission and they have narrow emission peaks. The last method is a combination of fluorescence imaging and information obtained from cell population in live animals. Fluorescence imaging was added to cell counting flow cytometer to create in vivo imaging. With this method fluorescently labeled cells are imaged in live animals.[1] Laser guidance is a method in which cells are drawn into the beam of the laser and propelled along the axis. Due to the use of fluorescence markers in flow cytometry it cannot be used to detect and causes some restrictions. Optical property changes occur due to changes in size, shape internal structure, or composition of a cell therefore changing the optical force exerted on the cell by the laser beam.[2] By using a combination of flow cytometry, laser guidance, and digital imaging it is aimed to create a fluid stream of cell particles with the laser that can be examined and sorted at the end of the channel.

Materials and Methods

A program to analyze the cells flowing through the channel was created. The program integrates previous programs to locate a particle and find its radius. It uses gradient analysis, edge detection, and curve fitting to locate the particle. Centroid analysis is then used detect the particles current location in the image. A combination of the information obtained from the curve fitting and centroid analysis are used to find the radius of the cell. Images collected from previous laser guidance experiments were used to test out the program. The images were collected using image correlation with multiframe particle tracking.

Results and Discussion

The program at the moment only looks at one image that has already been cropped to the particle. At the end it gives back the radius of the particle. The values seem to vary and the radius is not consistent when running the program. This may be due to calculation method that is used to determine radius. Further modifications will need to be done to perfect the program so that a consistent value is given. Another program that has already been created will be integrated into this one so that it will be able to find the velocity of the particle as it travels through the channel.

Conclusions

Further work will be done to the program so that it will be able to find a particle with other fragments in the picture. From there the program can be added to a flow channel in which it in vivo flow cytometry can be done. The next program to be added currently uses a series images to analyze particles and sort them, in the future applications can observe using movies to analyze the particles.

References

Faumont, F., Lockey, S., Rondeau, G., and Zemek, John 2008 Imanging a Moving Target. Biophotonics International. 28-31

[1]Hogan, H., 2006 Flow Cytometry Moves Ahead. Biophotonics International 38-42

[2]Ma, Z., Burg, K.J.L., Wei, Y., Yuan, X., Peng, X., Gao, B. 2008 Laser-guidance based detection of cells with single-gene modification. American Institute of Physics

[3]Ravinc, D.J. Tsuda, A., Turhan, A., Pratt, J.P., Huss, H.T., Zhang, Y. and Mentzer, S. 2006 Multiframe particle tracking in intravital imaging: defining Lagrangian coordinates in the microcirculation. Biotechniques 597-601

Acknowledgements

I would like to thank my advisor, Dr. Bruce Gao and graduate mentor Zhen Ma for their assistance and guidance on my project. Susan Lasser and SCAMP for part of my funding. And finally Clemson University and the BBSI and SSBR programs for the opportunity to do research this summer and also funding.

The Effect of Radiation on Mechanical Properties of Bone

Sosdian, L.[1] Kennedy, M.[1]
Department of Bioengineering [1] Clemson University, Clemson, SC, USA

Introduction: Bone loss is a serious obstacle for the future of long-duration space flight along with other deleterious effects that include both microgravity and ionizing radiation components.[1] NASA's current exploration roadmap describes a return to the Moon in preparation for more determined and extended Mars exploration in upcoming years.[1] Spacecraft shielding can somewhat reduce radiation exposure, but not completely down to relatively harmless levels. Unexpected solar flares and coronal mass ejections are of particular concern during lunar and other space-related missions.[1] This study investigates the effect that proton radiation has on mechanical properties of bone such as hardness and elastic modulus. Hardness is a measure of a material's resistance to plastic deformation and can be measured using a Microhardness Indenter.[3] The Modulus of Elasticity is defined as the stress/strain in the linear region of the curve of an ordinary tensile or compressive test and can be measured using a Hysitron Triboindenter Nanointenter.[2] Bone regeneration is an important concept that was taken into account when designing a testing procedure. The two main types of cells that function in bone growth are osteoblasts (responsible for the formation of bone) and osteoclasts (bone destroying cells).[2] During remodeling, it is common for the shape of the bone to change due to the fact that bone may be added to the periosteal (outer) or endosteal (inner) surfaces.[2] Due to the fact that the age of bone is different on the outer edges than in the middle, it was hypothesized that the radiation would affect the bone differently in these two regions.

Materials and Methods:

There were a total of 12 samples of female femurs (8 control and 4 proton radiation). 2Gy of radiation was administered for a total of 113 days. The samples were embedded in PMMA in sets of 6 and the top was determined to have been previously polished. For the Nanoindenter, a 5mm layer from sample #8 was cut using the Bueller Isomet Saw 4000. Individual samples were cleaned with ethanol. Using the Vickers Indenter, 5 rows of 5 indents were taken on the control samples and the proton radiation samples [Test force=.098 N, Dwell Time=15 sec]. A proton radiation sample was then tested using the Nanoindenter. Vickers indents were used as a guide and a group of nanoindents were taken in the middle of the bone and along one of the outer edges [Quasistatic mode: 3 segments, 5 sec each, max force=1000μN, load control]. The hardness using the two machines was compared to track hardness versus growth after radiation exposure.

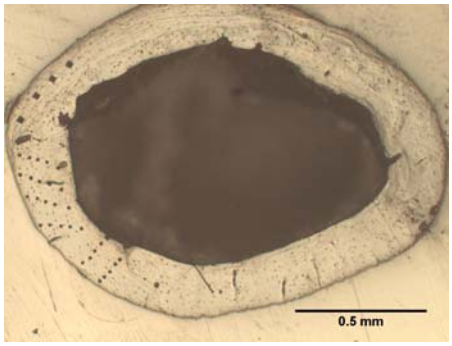

Figure 1: Control sample after Vickers Indents were taken

Proton Radiation (505)					
LLU- Indents (.49N) LLU- Hardness Calc		LLU -Indents (.49N) CU-Hardness Calc		CU-Indents (.49N) CU-Hardness Calc	
AV HV	76.5	AV HV	70.2	AV HV	65.5
STDEV	1.70	STDEV	1.20	STDEV	7.01
Control (497)					
LLU- Indents (.49N) LLU- Hardness Calc		LLU-Indents (.49N) CU-Hardness Calc		CU-Indents (.49N) CU-Hardness Calc	
AV HV	75.3	AV HV	71.2	AV HV	61.2
STDEV	1.90	STDEV	1.77	STDEV	5.70

Table 1: Hardness Calculations for Vickers indents by CU and LLU

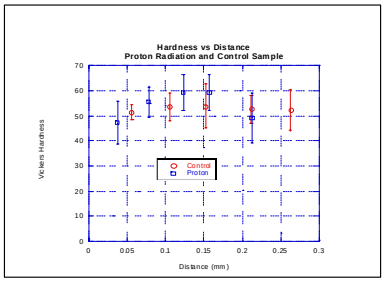

Figure 2: Hardness vs. Distance Graph for a proton and control sample

Table 1 shows measurements of previous Vickers indents compared to measurements at the start of this experiment. The Vickers indents on the proton radiated samples showed higher hardness values in the middle of the cross section than on the edges while the controls demonstrated a relatively constant hardness throughout the sample (figure 2).

Discussion and Conclusions: Both the Nanoindenter and the Vickers Indenter produced data that suggests the hardness of bone is higher in the middle of the cross section after radiation. This is consistent with the bone regeneration process where bone is added and broken down on the edges of the bone. However, due to the fact that the standard deviation was so large in all of the tests, two sample T-tests were performed on the Vickers and Nanoindenter data (outside vs. middle) and no difference between the data sets were found, indicating that the data gathered could be due to random chance. Future work for this experiment could include taking more data from different samples and analyzing the standard deviation and hardness trend. If the trend stayed the same, it would be reasonable to conclude that radiation does affect bone growth due to the fact that higher hardness values are found on the middle of the cross sections that the outer edges.

References:

[1]Lloyd, S. A., Bandstra, E. R., Travis, N. D., Nelson, G. A., Bourland, J. D., Pecaut, M. J., et al. (2008). Spaceflight-relevant types of ionizing radiation and cortical bone: Potential LET effect? *Advances in Space Research : The Official Journal of the Committee on Space Research (COSPAR), 42*(12), 1889-1897.
[2]Currey, John D. Bones: Structure and Mechanics. Princeton: Princeton University Press, 2002. 35.
[3]Callister, William D., Jr. "Chapter 6: Mechanical Properties of Metals." Materials Science and Engineering. 7th ed. 2007.

Acknowledgements: Linda Jenkins for sample preparation help, I. Rook and B. Zimmerman for Nanoindenter training, and NASA for funding

Characterization of Chemically Stabilized Hydrogels for Tissue Engineering the Nucleus Pulposus

Pascal, R, Mercuri, J, Simionescu, D
Department of Bioengineering, Clemson University, Clemson, SC

Introduction

Intervertebral disc degeneration (IDD) leads to one of the largest health care burdens in society affecting 70-80% of the world's population. Conservative estimates in the U.S. indicate that IDD ranked 12th among all hospital diagnosis in 2006, resulting in an aggregate cost of over $7.6 billion to treat.[1] Traditional surgical treatment options have been used as a last resort and have focused on treating the symptoms but fail to address the cause, which is largely accepted to begin with degeneration of the nucleus pulposus (NP). We hypothesize that, with early intervention, replacement of the nucleus pulposus with a bioengineered device containing a cell-seeded, chemically stabilized hydrogel may help regeneration of healthy NP.

Materials and Methods

Hydrogel scaffolds were prepared by combining 4 mg/ml hyaluronic acid (Fluka), with 27mg/ml chondroitin sulfate (USB Corp.), and 40mg/ml α-elastin (EPC) in an 3mg/ml collagen Type I (PureCol, Inamed). Hydrogel components were added and mixed thoroughly on ice while maintaining neutral pH 7.4. Gelation of gels occurred following incubation of gels at 37°C for at least 1 hour. Gels subsequently underwent stabilization via sequential 24 hour treatments in 30mM EDC/ 6mM NHS followed by 0.15% Penta-galloyl-glucose (PGG).

Cell Viability/Proliferation on PGG treated Hydrogels

MTS and Live/Dead (L/D) assays were conducted at 3 and 6 day time points on gels that had been treated with PGG only and seeded with porcine NP cells.

Gel Resistance to Enzyme Digestion

To assess hydrogel component resistance to degradation, gels were incubated in a GAGase mixture (5U/ml Hyaluronidase & 0.1U/ml Chondroitinase ABC in 100mM Ammonium Acetate, pH 7.4), an elastase mixture (10U/ml elastase in 50mM Tris, 1mM CaCl and 0.02% azide, pH 8), or a mixture of MMP-2 &-9 (20mM Tris, 5mM CaCl, 150mM NaCl, 1mM APMA, MMP-9, MMP-2) for 48-72 hours at 37°C. Non-digested (buffer only) samples were used as controls for comparison. Resistance to GAGase, elastase, and MMP digestion was assessed via DMMB assay for GAGS, mass loss, and SDS-PAGE analysis, respectively.

Results and Discussion

MTS data for PGG treated gels indicates a 3-fold increase in the number of cells present from the 3 to 6 day time point (figure 2). L/D pictures of day 3 show live cells present on the PGG treated gels. When comparing the L/D pictures for day 3 and 6, the cells are found within the gel in the day 6 pictures as opposed to just the surface as seen for day 3 (figure 1). Initial analysis of the gel morphology during MTS and L/D indicated that the gels were soluble and degraded over time despite PGG treatment.

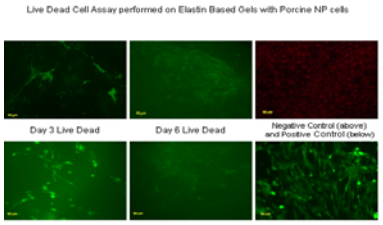

Figure 1

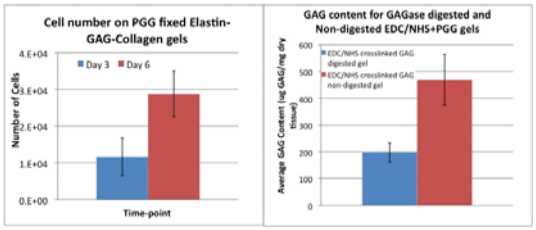

Figure 2

In an attempt to minimize gel degradation an EDC/NHS crosslinking mechanism was introduced and gel component resistance to degradation was assessed. The results from the GAGase digestion show that there was a statistically significant ($p<.001$) decrease in GAG content for EDC/NHS+PGG digested gel compared to the non-digested gel. This indicates that EDC/NHS+PGG does not effectively stabilize the GAG component of the gel. Results from elastase digestion shows a minimal mass lost due to the enzyme (10.49%) however there remains significant mass loss due to solubility of the elastin component (figure3). Mass loss and SDS-PAGE results for MMP are pending.

Sample	Average % mass loss	% Mass loss due to elastase digestion
EDC/NHS+PGG stabilized elastase Non-Digested Samples	67.15	10.49
EDC/NHS+PGG stabilized elastase Digested Samples	77.64	

Figure 3

Conclusions

1) Elastin-GAG PGG treated hydrogels are not cytotoxic and support NP cell proliferation.
2) EDC/NHS+PGG treatment of hydrogels did not fully stabilize GAGs.
3) The Elastin component appeared to be stabilized by the EDC/NHS+PGG treatments.
4) Further studies are warranted to enhance hydrogel stabilization

References

[1]AHRQ. Healthcare Cost and Utilization Project (HCUP) Database. http://www.ahrq.gov/data/hcup, July 18,2009.

Acknowledgements

Funding from NIH/INBRE summer supplement award and BTRLab.

High Speed Kinematic Video Analysis of a Unicompartmental Replacement During Simulated Gait

Roach, B[1], Matheny, J[1], Spinelli, M[2], Blob, R[1], DesJardins, J[1]
[1] Clemson University, Clemson, SC, USA
[2] Rizzoli Institute, Bologna, Italy

Introduction: Total knee arthroplasty (TKA) continues to increase in use since its first introduction nearly thirty years ago[1]. TKA provides the patient correction of deformity, restoration of joint mobility and relief of pain. While a total knee replacement (TKR) is successful, it is sometimes possible to achieve joint maintenance with the use of less invasive unicondylar systems, whereby only one condyle need be replaced. The soft-tissue constraints and kinematics of these uni-condylar systems is largely uninvestigated, however. In this study a novel method of analyzing the kinematics of implant motion was implemented using high speed video analysis. After experimental model validation, this method is used to quantify the effect of siimulated ligament configurations uni-condylar system implant kinematics.

Materials/Methods: The Instron/Stanmore Knee Simulator (University College London, London, England) was used to replicate a gait cycle of 1 Hz, complying with ISO standard 14243-1. Size maxi, ultra high molecular weight polyethylene (UHMWPE) uni-condylar inserts, and unicondylar stainless steel components (Citieffe, Bologna, Italy) were used. The tibial tray was instrumented with discrete 2mm diameter markers in the superior and lateral views, and a high speed video camera system (Vision Research, Inc., Wayne, New Jersey) was positioned above the simulator to record the motion of each station. Camera settings were such that the frame size was 1,024 x 1,024 pixels, with a frame rate of 250 frames/second. After recording data, it was exported to computer software (dltViewer, Matlab, Durham, North Carolina) where the movement of the tibial markers could be digitized. The tibio-femoral lowest-contact points in the xy plane were calculated and used to compare the motion paths for each soft tissue configuration. 6 configurations in all, they were labeled SoftAP, HardAP, SoftPC, SoftPHardA, Soft wGap, and Hard wGap to correspond with soft A & P – 2.5 mm gaps A & P, hard A & P, soft pre-compressed, soft P – 2.5 mm gap and hard A, soft A – 2.5 mm gap and hard P, and hard A & P – 2.5 mm A & P gap, respectively. Statistical differences were compared using analysis of variance (ANOVA) with Games-Howell post hoc tests for inequality of variances ($\alpha = .05$), as well as paired t-tests to confirm differences.

Results: Based on known distances between reference markers in the field of view and known pixel resolutions, the accuracy for the presented method was found to be .19 ± .01 mm/pixel for the 4 stations recorded. A typical graph of the tibio-femoral contact path during simulated gait is found in Figure 1. This represents a patient with normal anterior and posterior cruciate ligaments. Correlations of the data from the motion path for each configuration were separately calculated; these showed that all four stations performed similarly for a given orientation ($r=0.99\pm.01$). ANOVA of the natural log of the motion path data (data was transformed to reduce variance) showed significant differences existing among configurations ($F=47.856$, $p-=0.000$).

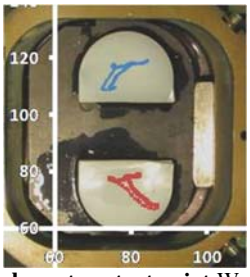

Figure 1: The lowest contact point Wear path for one simulated gait cycle of normal ligamental configuration (axes are in mm).

Games-Howell post-hoc tests were used for non-equality of variances followed by dependent t-tests to confirm the results ($\alpha=0.05$). T-tests demonstrated 13 pairs of configurations whose paths were significantly different (see Table 1).

Table 1: Paired t-test results for all configurations.

	SoftAP	HardAP	SoftPC	SoftP HardA	Soft wGap	Hard wGap
SoftAP		.000	.170	.000	.000	.000
HardAP			.000	.000	.588	.002
SoftPC				.000	.000	.000
SoftP HardA					.000	.004
Soft w. Gap						.002

Conclusion: It can be seen from the graph in Figure 1 that this method of analysis not only generates accurate results but it also provides visual confirmation of the tibio-femoral contact path. In addition to the onboard capabilities of the Stanmore Instron Knee Simulator, this high speed video analysis method can generate position of the contact path in the medial/lateral direction as well as the anterior/posterior. The capacities of the dltViewer software create an accurate interpretation of the contact path motion between the femoral component and tibial insert, displaying a visual aid capable of aiding modularity in implant systems, and potentially aid in surgical implantation itself. The ability to graphically and visually model this path will ensure patient and surgeon confidence, leading to greater customization of implants to fit the needs of individual patients. The results from the ANOVA and paired t-test support the initial assumption that the six configurations differ from one another as well as validating the use of tracking for determination of generated wear paths via different ligamental configurations.

References: [1] Kaper BP, et al... Medium-term results of a mobile bearing total knee replacement. ClinOrthop 1999; 367:201-9.

Acknowledgments: The authors would like to thank the Department of Bioengineering at Clemson University for their support.

Exploration, Development, and Implementation of the Clemson University Implant Retrieval Program (CUIRP)

Wabler, M, Alvarez, E, DesJardins, J
Department of Bioengineering, Clemson University, Clemson, SC

Introduction

Prosthetic devices for fracture fixation and total joint replacement have become more reliable in recent decades, leading to a steady increase in their use and success in the treatment of arthritis, deformities, and chronic joint pain [1]. While most total joint replacements are permanent, complications during a prosthetic's lifetime can arise that lead to revision, or in severe cases, complete removal of the implant [2]. Explantation and characterization of such devices can lend valuable information on its in vivo functional performance, long-term structural and material properties, and failure modes. This abstract describes the implementation of a state-wide implant retrieval program to assist surgeons and bioengineers in the collection of this information to enhance implant longevity.

Materials and Methods

In accordance with all approved Clemson University and local hospital IBC and IRB protocols, all implants were explanted at Greer Memorial Hospital and Patewood Memorial Hospital, both affiliated with the Greenville Hospital System, Greenville, SC. With consent of the patient, the implants were removed from the operating room by the physician's assistant on duty and taken to a non-sterile cleaning area. Implants were then washed lightly with water to remove any tissue debris that might remain from the patient, placed in supplied formalin containers, and labelled appropriately with an attached patient data sheet which details physical information (height, weight, etc.), reasons for explantation, and implant information (make, scratching, etc.) A qualified representative then transported the containers back to Clemson University for analysis. Implants were catalogued via assignment of a number that matches the implant to its proper information packet. Following the cataloguing step, implants were stored in the formalin containers for a period of no less than two weeks. When the two week period had lapsed, the implants were taken to the Clemson University Histology lab for a preliminary cleaning with deionized water and soft brushes. This process removed remaining tissue, and was followed by further cleaning in an ultrasonic bath. Photographic documentation of the clean implant was taken, and components were placed in boxes for storage.

Figure 1:Acetabular shell, polyethylene liner, and femoral component of a retrieved implant

Implants were visually examined and macroscopic evaluation was performed. The examiner recorded any possible wear, scratching, shape change, mechanical damage, embedded particles, calcification, and other properties that may have led to mechanical failure. The results were rated on a severity scale ranging from none to severe. Implants were then ready to be analysed using a series of techniques such as Optical Microscopy, X-ray Absorption Spectroscopy, Gravimetric and Volumetric Wear, Surface Damage Mapping, and Mechanical Testing. Questions that are specific to an individual implant can be investigated directly, and long-term trends in implant materials, designs, and manufacturing methods can be investigated following the collection and analysis of multiple implants within a dataset.

Results and Discussion

Five implants have been obtained thus far, all total hip components consisting of stems, femoral heads, liners and shells.

Figure 2: An illustration of total hip and total knee replacement components

Manufacturers include Smith & Nephew, Biomet, Zimmer, and DePuy. Reasons for explantation or revision have thus-far varied, and include fracture, infection, and loosening.

Conclusion

The Clemson University Implant Retrieval Program (CUIRP) has successfully obtained five implants in cooperation with Dr. Brian Burnikel of the Greenville Hospital System. CUIRP hopes to speak with 4 more doctors of the Greenville Hospital System in early August to increase the number of implants obtained and begin the collection of knee retrieval implants. The program is also hoping to launch an international arm in cooperation with a doctor from Austria. It is hoped that the creation of this retrieval program will help students and physicians around the country learn and improve on implant durability and design.

References

1. Grupp, TM, et al. "Fixed and mobile bearing total knee arthroplasty…" Clinical Biomechanics. 24 : (210-217).
2. Ingham, E, et al. "Biological reactions to wear debris in total joint replacement." Proceedings of the Institution of Mechanical Engineers Part H. 214 (21-37).

Design of an Ankle Motion System for an Ankle-Foot-Orthosis Testing Apparatus

Warrick, T[1], Benson, D.[2], Brooks, R.[2], Skewes, E[2], DesJardins, J[1],
[1] Clemson University, Clemson, SC, USA, [2] Shriners Hospital, Greenville, SC, USA

Introduction

An Ankle Foot Orthosis (AFO) is a brace used in the correction of many gate related problems such as drop foot. AFOs are tailored to individual patient needs, and can range from stiff and rigid to flexible and articulated. A common challenge with the stiff AFOs is where to make the cutline in relation to the malleolus to achieve an appropriate stiffness for the patients needs. The goals of this study were 1) to construct a user-friendly apparatus that is capable of reproducibly testing the AFO stiffness vs. AFO design parameters in terms of physiologic torque and angular rotation, and 2) to determine the effect of different AFO malleolus cut lines on the resulting stiffness of AFOs for enhanced patient fit and function.

Materials and Methods

The AFO testing apparatus was constructed to replicate the motion of the ankle as closely as possible. The apparatus can replicate the key ranges of motion: dorsiflextion/plantarflexion (+20°/-50°), inversion/eversion (+20°/-40°), and adduction/abduction (+10°/-20°), with the ability to isolate or combine these ranges of motion as desired. Adjustments can be made on the apparatus to accommodate a large range of AFOs, from child to adult sizes, while ensuring the axis of rotation passes through the center of the ankle.

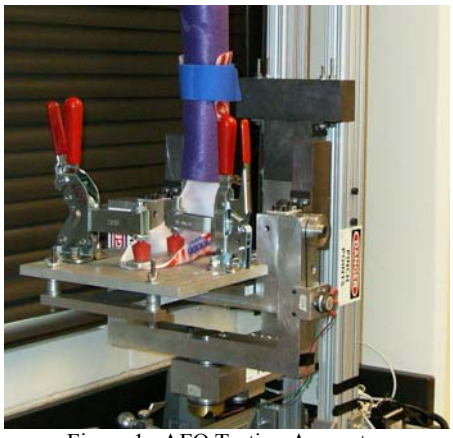

Figure 1. AFO Testing Apparatus

Three Novotechnik P2501 potentiometers with a resolution of 0.01° and an independent linearity of +/- 0.2% stream voltage signals into LabVIEW where they are converted into degrees of rotation. A Transducer Techniques SWS250 torque cell (250 ft-lb range) with an accuracy of +/- 0.25 ft-lbs streams voltage signals to a Transducer Techniques TMO-2 signal conditioner then into LabVIEW where it is converted into torque in [ft-lbs]. The signals are graphed on a rotational torsion graph where information about the stiffness of an AFO is related to the slope of this curve. Raw data is assessed for measures of stiffness, maximum torques, ranges of motion, and loading hysteresis.

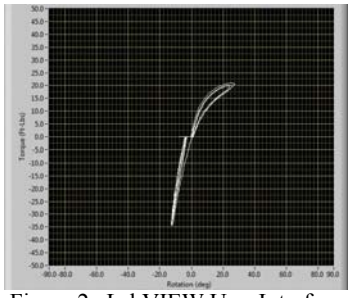

Figure 2. LabVIEW User Interface

Results

As can be seen in Figure 2, there is some hysteresis in the rotational torsion curve, represented by the loop that is formed [1]. The slope of the average of the torques values at the top and bottom of the loop at each degree of rotation is the stiffness of the AFO [1]. The integral of the area inside this loop is the energy absorbed by the thermoplastic material of the AFO during deformation [2]. The operator will follow set standard operating procedures to ensure the tests are repeatable and reduce the human error incurred during the tests.

Data Analysis

The LabVIEW program collects the angle and torque measurements, the slopes of the graphs, and the information relating the angle measurements to the maximum torque values. The output of the LabVIEW program is a data file that can be imported into Microsoft Excel for further analysis. The data will be processed following detailed standard operating procedures to produce useful information about the stiffness of each AFO such that a system which will benefit physicians.

Conclusion

Data collected during tests will be used to quantify different cut lines of AFOs with a future goal of being able to associate cut line numbers with patients. Meaning, when a patient comes in who presents similar symptoms as another patient, the physician will be able to look up the cut line used on the other patient and produce a similar AFO for the current patient. Since no patient is exactly like another, each AFO will continue to be fabricated for the needs of the individual patient, but the physician will have a benchmark to start with rather than complete trial and error.

References

1. Singerman, et al. JPO, 1999. Vol 11, Num 3, p 48.
2. Novacheck, et al. JPO 19-4A.

Acknowledgments

The following people are thanked for their design assistance with the AFO testing apparatus: Shea Bielby, Barret Hutto, Matt Manning, Dev Raghavan, Daniel Reed, Laila Roudsari, Laura Reese, Leslie Sierad, Shelby Skoog, and Betsy Tedder.

Drug Delivery Strategies for Treating Cardiac Dysfunction Following Myocardial Infarction

Sy, J.C.; Murthy, N.; Davis, M.E.
Georgia Institute of Technology and Emory University, Atlanta, GA USA

Abstract
Heart disease remains the leading cause of death worldwide, accounting for more than one in ten deaths in recent years. While heart disease encompasses a range of disorders, cardiac dysfunction following acute myocardial infarction (MI) accounts for a large fraction of deaths in developed countries. Following MI, an insufficient endogenous healing response triggers an inflammatory response that eventually leads to scarring and loss of contractile heart function. Researchers have explored a variety of avenues to achieve cardiac regeneration – including pharmacological agents, cell therapy, and mechanical devices – with varying levels of success. This work focuses on the development of drug delivery vehicles designed to reduce the inflammatory response and deliver appropriate cues for regeneration.

One of the key developments in drug delivery has been the development of sustained release formulations from degradable polymeric devices. Current FDA-approved formulations rely on poly(α-hydroxy acids) such as poly(lactic acid), poly(glycolic acid), and their copolymers. These polymers degrade into acids that are readily cleared by the body's metabolic processes. However, the acidic degradation products of the polymers may not be suitable for treating inflammatory diseases, such as cardiac dysfunction following MI, since the drop in pH may exacerbate existing inflammation. Polyketals are a new class of biodegradable polymers that are based on the acid-sensitive ketal linkage in the backbone. These polymers degrade into diols and acetone, which do not directly affect the local pH. Furthermore, a number of diols are on the FDA's list of compounds generally regarded as safe (GRAS) while acetone endogenously metabolized by the body. Due to these properties, polyketals have distinct advantages for treating inflammatory diseases, where a drop in pH is undesirable.

The feasibility of using polyketals as drug delivery vehicles *in vivo* was tested in a rodent model of cardiac dysfunction. Poly(cyclohexane 1,4-diylacetone dimethylene ketal) (PCADK) was used to encapsulate SB239062, an anti-inflammatory drug that inhibits the p38 MAPK pathway. Large (~20 μm diameter) microparticles were fabricated and directly injected into the infarcted region of rat hearts that had undergone permanent occlusion of the left anterior descending coronary artery. Biochemical analyses of heart tissue show that activation of p38 MAPK and its downstream effects were reduced by the treatment for at least one week. More importantly, rats treated with SB239063-loaded microparticles showed significantly improved heart function three weeks following surgery when compared to a similar PLGA control. We hypothesize that the sustained inhibition of p38 MAPK resulted in a microenvironment that fostered cardiac regeneration rather than scarring of the ventricular wall. Quantification of fibrosis in the heart at three weeks showed that animals treated with SB239063-loaded PCADK microparticles had significantly lower levels of collagen deposition compared to control groups. These data suggest that carrier chemistry affected the outcome of cardiac regeneration.

While data suggests that p38 signalling was inhibited the first week following surgery, no functional improvement was seen until 21-days post-surgery. We hypothesize that this may be due to the role in p38 in late-stage fibrosis. In order to treat more immediate effects of MI, we are currently exploring functionalizing microparticle surfaces with nitrilotriacetic acid-Ni (NTA-Ni) in order to bind His_6-tagged proteins. This immobilized metal affinity chromatography (IMAC) inspired functionalization will give the ability to deliver both short acting growth factors which can work in concert with anti-inflammatory treatment to foster cardiac regeneration. Microparticles containing the NTA moiety were fabricated by introducing a NTA-conjugated lipid in our microparticle formulation.

Using His_6-tagged GFP as a model protein, we are able to load microparticles with therapeutically relevant doses of proteins (~1000 ng/mg particle). Release studies show that the protein is rapidly released ($t_{1/2}$ = 2h) from the surface in physiological, serum-containing conditions. IMAC-functionalization has a number of advantages over traditional techniques for loading protein into microparticles. First, the risk of protein denaturation is diminished as proteins are not exposed to organic solvent during particle loading. Proteins can also be loaded at low concentrations at relatively high efficiencies (~40% loading while using 100-1000 ng/ml of protein). Displaying proteins in their native state on the surface of a microparticle also raises the possibility of using NTA-Ni interactions to target proteins to specific cellular surface markers. *In vitro* tests show that VE-Cadherin loaded particles bind to endothelial cells (VE-Cadherin positive) at a two-fold greater frequency compared to cardiac myocytes (VE-Cadherin negative) or other negative controls. Given the large number of proteins already routinely expressed with the His_6-tag, we anticipate a number of different uses for IMAC functionalized microparticles.

Developments in new biomaterials and drug delivery strategies have the potential to improve patient outcome. We present here a new class of degradable polymers for drug delivery applications with particular strengths in treating inflammatory diseases. In addition, we introduce a technique to add NTA functionality to the surface of polyketal microparticles in order to use His_6-tagged proteins as controlled release therapeutics as well as potential targeting agents for microparticles.

Acknowledgements: JCS has received graduate fellowships from the NSF and the Department of Homeland Security. This work was funded by grants to MED and NM from the NIH.

A New Reactive Oxygen Species Sensitive Delivery Vehicle for Targeting Oxidative Stress

D. Scott Wilson and Niren Murthy.
The Wallace H. Coulter Department of Biomedical Engineering
Georgia Institute of Technology

of Purpose: Oxidative stress, a cytopathic consequence of excessive production of reactive oxygen species (ROS) is implicated in the development and persistence of many inflammatory diseases, including inflammatory bowel disease, acute lung injury, and myocardial infarct. In this presentation, we introduce a new ROS-sensitive drug delivery vehicle, formulated from Poly(Thioketal) polymers (PTK), that has the ability to selectively release therapeutics inside cells under oxidative stress.

Methods: Poly(Thioketal) Polymerization. A schematic of the stepwise polymerization of cyclic and aliphatic dimercapto-monomers and 2,2-dimethyoxy propane (DMP) used to make PTKs is shown in Figure 1(A). A 3-neck flask was charged with equimolar amounts of the dimercapto-monomer and DMP dissolved in distilled benzene. This stirred solution was heated to 107°C before the addition of a catalytic about of *p*-toluenesulfonic acid. As the reaction proceeds at 107°C, methanol, benzene, and unreacted DMP are collected via distillation. In order to compensate for the removal of DMP and benzene from the reaction flask, DMP and benzene are added drop-wise throughout the duration of the reaction (24hrs).

Microparticle Formulation. Protein and small molecule-loaded thioketal microparticles (TKMP) were prepared by w/o/w (water/oil/water) double-emulsion and o/w single-emulsion methods. For the protein-loaded particles, a primary w/o emulsion is created by dispersing 100µL of FITC-labeled OVA albumin aqueous solution (20mg/mL) in an organic phase consisting of 100.0 mg PTK dissolved in 1.0 ml dichloromethane (DCM). This primary w/o phase is then added and dispersed by homogenization in a secondary aqueous solution containing 5% (w/v) surfactant to produce the final w/o/w emulsion. This w/o/w emulsion is then stirred under vacuum to remove the DCM. The particles are then isolated via centrifugation and lyophilized.

Polymer Degradation. PTKs were dissolved in DCM containing a phase transfer catalyst and potassium superoxide. After 8 hours the DCM was evaporated and the resulting polymer residue analyzed via gel permeation chromatography.

Intracellular Dye Release. RAW-264.7 macrophages were treated with empty TKMPs or TKMPs loaded with the hydrophobic dye CMFDA. The cells were incubated with the particles for 4 hrs before being washed 3 times with PBS. The particle-treated and untreated cells were then given fresh media or media containing 1.0 µg/ml of lipopolysaccharide (LPS). LPS is an endotoxin known to activate macrophages and lead to the overproduction of the ROS superoxide. After 12 hours, the cells were then assayed for intracellular dye release by flow cytometry.

Results: PTKs synthesized according the schematic show in Figure 1(A) had number average molecular weights between 2,000 and 4,000 Da. Exposure of these polymers to potassium superoxide reduced the molecular weights to below 700 Da; however, polymers showed excellent stability to aqueous solutions with pH's of 1.0 and 10.0.

An SEM image of the OVA-loaded microparticles formulated from PTKs is shown in Figure 1(B). The florescent microscopy image of these particles verifies encapsulation of OVA in the particles.

Flow cytometry performed on cells receiving empty and CMFDA-TKMPs show an increase in the amount of dye released into cells that have been stimulated to overproduce superoxide by the addition of LPS. The red line in Figure 2 represents an increase in dye released in cells treated with CMFDA-TKMPs and LPS over the green line representing cells that only received CMFDA-TKMPs.

Conclusions: In this presentation, a new class of ROS sensitive polymers was synthesized from dimercapto-monomers and 2,2-dimethyoxy propane. PTKs were used to formulate small molecule and protein-loaded microparticles. Cell culture experiments demonstrate that dye-containing microparticles formulated from PTKs release their payload more rapidly in cells that overproduce superoxide. These results demonstrate the ability of TKMPs to target therapeutics to cells that overproduce the ROS super oxide.

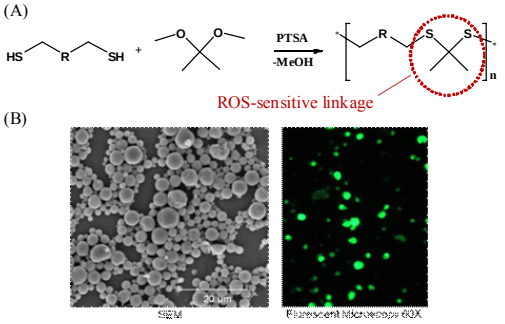

Figure 1. PTK, a new ROS-sensitive drug delivery vehicle: (A) PTKs are synthesized from dimercapto-monomers and DMP, (B) SEM and florescent microscopy images of TKMPs loaded with fluorescently-labeled OVA albumin.

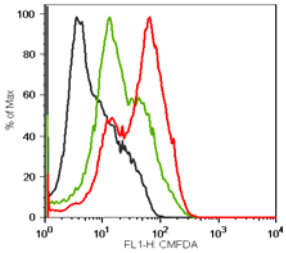

Figure 2. TKMPs target release in cells that overproduce ROS. Flow cytometry performed on RAW 264.7 macrophages treated with empty TKMPs and LPS (black), CMFDA-TKMPs (green), and CMFDA-TKMP and LPS (red) show that TKMPs have faster release kinetics in cells that have elevated levels of ROS (i.e. LPS treated cells).

Funding: The Center for Drug Discovery, Development, and Delivery (CD4), and NIH CETENG Training Grant

Electrophoretic Deposition of Silica-Calcium Phosphate nano Composite on Ti-6Al-4V

Aniket, Ahmed El-Ghannam

The University of North Carolina at Charlotte, Charlotte, NC, USA

INTRODUCTION: Tissue integration between bone and orthopedic implant is essential for implant fixation and longevity. Fibrous encapsulation of the metal implant results in micro-motion and implant failure. Coating orthopedic implants with bioactive ceramics facilitates implant-bone bonding and hence better fixation. Various bioactive ceramics have been used for coating with limited success due to instability of the ceramic/metal interface. The use of techniques such as plasma spraying has limited applicability on coating porous substrates besides decomposing the ceramic and deteriorating its bioactivity and stability. The objective of the present project is to coat the surface of medical grade Ti-6Al-4V orthopedic implants with bioactive ceramic to improve tissue adhesion and implant fixation. Silica-calcium phosphate nano composite (SCPC) is a novel bioactive resorbable ceramic that has the ability to bond to bone and expedite bone formation. Moreover, SCPC has demonstrated superior mechanical properties, bioactivity and resorbability compared to traditional calcium phosphate ceramics and bioactive glass. The present study demonstrates the successful coating and characterization of SCPC on Ti alloy implants using Electrophoretic Deposition (EPD) technique. The effects of SCPC's composition, zeta potential and conductivity as well as EPD parameters such as voltage, suspending medium, pH and deposition time on the coating process were investigated. Moreover, the effects of Ti alloy surface modifications and thermal treatment on the adhesion strength at the interface between SCPC and Ti alloy were determined.

MATERIALS AND METHODS: Three different chemical compositions of SCPC – SCPC25, SCPC50 and SCPC75 containing calcium phosphate/silica components in the weight ratio of 75/25, 50/50 and 25/75 respectively were prepared. The ceramic was sintered at 850ºC for 2 hours, ground and sifted to particles in the size range 50 nm - 10 μm. Zeta potential and conductivity measurements were performed in the pH range 2 – 9 by suspending 1.5 mg of SCPC particles in 15 ml of 50% (v/v) ethanol in water. Similar experiments were performed in pure ethanol and DI water. SCPC50 particles were suspended in pure ethanol and used for EPD. Flat Ti alloy discs were subjected to surface modifications by immersion in either 34% HNO_3 for 40 min at 65 ºC (passivation) or 7.5N NaOH for 24 hrs at 60 ºC. For EPD, the Ti alloy discs to be coated served as the anode while a similar Ti alloy disc was used as the cathode. The concentration of the SCPC suspension was varied from 2 – 7.5% (w/v) and various coating durations from 30 to 600 sec were tested using a deposition voltage from 30 to 120V. The SCPC coated Ti alloy discs were subjected to thermal treatment at 600 ºC, 700 ºC or 800 ºC under argon and the coating morphology was analyzed using SEM. Adhesion strength was measured according to ASTM standard (F1147-05) using an Instron testing machine and fracture surface analyses was carried out using SEM-EDX. The SCPC coated Ti discs were immersed in 75 mL of physiological solution for 7 days and analysed for adhesion strength. Statistical analysis for adhesion strength under different conditions was performed using student's t-test with $p < 0.05$. Porous alloy discs were then coated using the optimized process and cold mounted in epoxy. Multiple cross-section analyses of porous Ti discs were carried out to determine the coating thickness in various regions of the discs.

RESULTS: Among the different SCPC compositions tested, SCPC50 exhibited maximum zeta potential (-41 mV) and lowest conductivity (2 μS/cm) in pure ethanol and was therefore chosen for EPD. A uniform SCPC layer with 100 % coverage could be deposited on passivated Ti alloy surface using 5% (w/v) SCPC suspension and a voltage of 50V for 3 min. Tensile testing showed that the adhesion strength between SCPC and Ti alloy after thermal treatment at 800 °C was 47 ± 4 MPa which was higher than the ASTM standard requirement of 30 MPa. Fracture surface analyses using SEM-EDX revealed that the failure was largely contained within the polymer or the ceramic layer, suggesting a strong ceramic-metal interface. The interface between the ceramic and metal appeared to be very intact. After 7 days immersion in physiological solution, SCPC enhanced the deposition of a biological hydroxyapatite layer on its surface. Mechanical testing showed that the fracture occurred at the interface between hydroxyapatite and the SCPC layer at 6.4 ± 1.8 MPa. SEM analyses of various sections of SCPC coated porous Ti discs showed that after 30 sec coating, the entire surface as well as pores of the Ti alloy disc was covered with a uniform 4 μm thick SCPC layer.

CONCLUSION: A successful coating of a thin and homogenous layer of bioactive SCPC on the surface of Ti alloy orthopedic implant material was achieved using EPD. The SCPC layer was strongly adhered to the metal surface even after 7 days immersion in physiological solution. Moreover, the SCPC coating enhanced the deposition of a biological hydroxyapatite layer on the implant surface. Therefore, SCPC coating has the potential to expedite bone bonding to the metallic implant and enhance improve fixation.

Dielectrophoresis separation of colon cancer cell

Yang, F[1], Yang, XM[2], Jiang, H[3] , Wood, P[2], Hrushesky, W[2], Wang, GR[1].
[1]Dept. of Mechanical Engineering & Biomedical Engineering Program
[2]Center for Colon Cancer Research
University of South, Carolina, Columbia, SC 29208, USA
[3]GraceFlow Technology, Irmo, SC.

Abstract

Separation of cancer cells from the other biological cells and non-biological particles is important for clinical diagnostics. In this presentation, we use conventional dielectrophoresis (c-DEP) in a microfluidic chip to manipulate and collect colorectal cancer HCT116 cell. It is noticed that at particular AC frequency band, the HCT116 cell experience negative DEP force and are deflected to a side channel from a main channel clearly after the electric activation. This motion caused by negative DEP can be used to separate the cancer cell from others.

Figure 1 shows the visualization of the deflection of the colorectal cancer HCT116 cell of approximate 20 μm in diameter for separation to the side channel due to DEP force, with and without the electric activation..

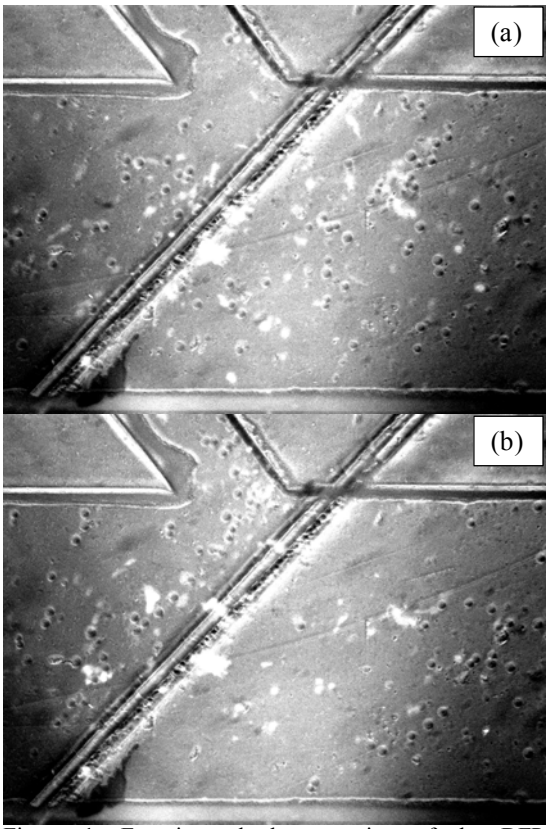

Figure 1. Experimental demonstration of the DEP deflection. (a) No AC activation and most colorectal cells move downstream of the main channel. (b) With AC activation, almost all colorectal cells were repelled to the side channel due to DEP force.

The voltage used in Figure 1(b) was 16Vp-p. The flow rate in Figure 1 was 0.1 μL/min. In Figure 1(a), approximately 90% of the colorectal cells flow downstream of the electrodes to the main channel without AC electrode activation. On the other hand, with the activation of the electrodes, almost all colorectal cells migrate to the side channel under DEP force as shown in Figure 1(b).

The DEP spectrum of the cancer cell is measured. Detail chip design, flow condition and the separation and collection efficiency are also investigated as well. (as shown in Figure 2. and Figure 3.).

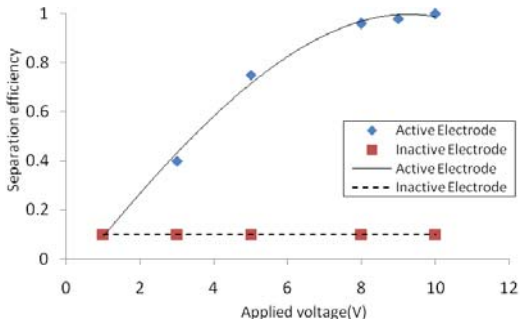

Figure 2. Separation efficiency as a function of applied voltage.

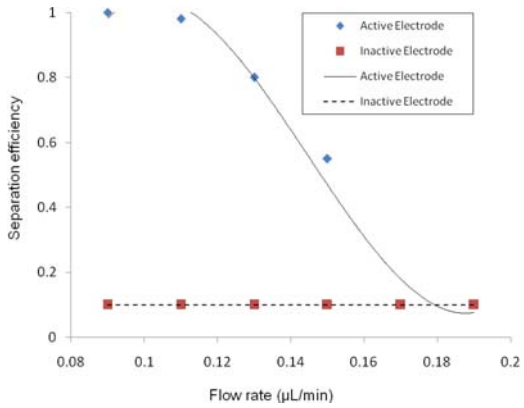

Figure 3. Separation efficiency as a function of sample flow rate.